



Article

Thermal Behaviour of Different Land Uses and Covers in the Urban Environment of the Spanish Mediterranean Based on Landsat Land Surface Temperature

Enrique Montón Chiva * and José Quereda Sala

Laboratory of Climatology, Interuniversity Institute of Geography, Universitat Jaume I, Avda. Sos Baynat s/n, 12006 Castellón, Spain; quereda@uji.es

* Correspondence: montone@uji.es

Abstract: Previous research has found higher temperature trends at urban observatories. This study examines in depth the features of the urban environment, the thermal behaviour of land use and land cover, and the changes that have taken place in five urban areas of the Spanish Mediterranean. The CORINE Land Cover database was used to delimit the primary land use land cover (LULC) and its changes between 1990 and 2018. Once this had been established, land surface temperatures (LSTs) between 1985 and 2023 were retrieved from the Landsat database available on the Climate Engine website. There has been a significant advance in artificial land uses, which have become the main uses in the urban areas in Valencia and Alicante. An analysis of the primary land cover showed the greatest thermal increase in artificial surfaces, especially in the industrial, commercial, and transport units that are common on their outskirts, without exception in any urban area. The results are less clear for urban fabrics and agricultural areas due to their diversity and complexity. The density of vegetation is a key factor in the magnitude of the UHI, which is higher in the urban areas with more vegetated agriculture areas, therefore showing lower LST than both industrial units and urban fabrics. Another important conclusion is the role of breezes in limiting or eliminating the strength of the UHI. Sea breezes help to explain the monthly variation of UHIs. Both bodies of water and areas of dense tree vegetation provided the lowest LST, a fact of special interest for mitigating the effects of heat waves in increasingly large urban areas. This study also concludes the different effect of each LULC on the temperatures recorded by urban observatories and enables better decision-making when setting up weather stations for a more detailed time study of the urban heat island (UHI).

Keywords: urban climate; land surface temperature; UHI; CORINE Land Cover; Climate Engine Project



Citation: Montón Chiva, E.; Quereda Sala, J. Thermal Behaviour of Different Land Uses and Covers in the Urban Environment of the Spanish Mediterranean Based on Landsat Land Surface Temperature. *Urban Sci.* **2024**, *8*, 147. <https://doi.org/10.3390/urbansci8030147>

Academic Editor: Aya Hagishima

Received: 3 August 2024

Revised: 16 September 2024

Accepted: 20 September 2024

Published: 23 September 2024



Copyright: © 2024 by the authors. Licensee MDPI, Basel, Switzerland. This article is an open access article distributed under the terms and conditions of the Creative Commons Attribution (CC BY) license (<https://creativecommons.org/licenses/by/4.0/>).

1. Introduction

Urban climate is a topic of unquestionable scientific interest. From a socio-demographic standpoint, although cities take up only a small part of land, over 50% of the world's population live in them [1], and it is expected that by 2050, almost seven out of ten people will do so [2]. Millions of people's health and wellbeing may be impacted by rising temperatures and the presence of pollutants [3–5]. Indeed, urban sprawl has a wide range of consequences for the environment due to the increase in paved surfaces, health, with rising mortality rates, and the economy, owing to higher energy demand [6]. For good measure, the urban climate also has a bearing on one of the scientific topics that has generated the largest number of studies, climate change. The aforementioned impact of urban climate on temperatures is an issue to be taken into account in relation to the climate change hypothesis. The principal observatories tracking the evolution of global temperatures are located in large and rapidly growing cities and have been affected by the occurrence of higher temperatures, known as the urban heat island (UHI), which is the biggest downside of urbanisation [7]. These two factors together have led to an exponential increase in research on UHIs in recent decades [8,9], especially since 2012 [10]. The topic and its beginnings

can, of course, be traced back to L. Howard's study of London in 1820 [11], more than two centuries ago, and there have been frequent reviews of articles on the subject [10,12].

The UHI is defined as the presence of higher temperatures in urban areas versus non-urban areas [13]. The latter areas, defined as rural, are a blend of distinct agricultural areas and equally diverse vegetation spaces in mid-latitude countries [14]. Higher urban temperatures are the outcome of the following two heat sources: firstly, urban structures that store and radiate the sun's heat, and secondly, anthropogenic heat sources [15]. Concerning the first source of heat, namely, solar heat storage and emission, urbanisation involves replacing soil and vegetation with impervious surfaces and urban structures [16]. Specifically, asphalt and concrete have a high thermal mass, streets bordered by tall buildings on both sides act as low-ventilation canyons, and air conditioners and vehicles are sources of heat [10]. Other authors rightly add the alteration of radiation exchanges between the surface and the atmosphere due to the rise in pollutants and aerosols [11]. A more comprehensive list of processes taking place in urban areas would include anthropogenic heat production; the reduction of latent heat loss due to paved surfaces, efficient drainage systems and sparse vegetation; little loss of sensible heat owing to lower wind speed; increased absorption of solar radiation in urban canyons; a decrease in outgoing long-wave radiation; increased heat storage in building materials caused by their high capacity to retain heat during the day and release it at night; and the re-emission of atmospheric long-wave radiation to the ground due to the greater presence of pollutants [17].

Satellite imagery is an outstanding resource for studying UHIs to such an extent that most of the recent research on this topic has tapped into it [11]. GOES data have been harnessed to study the urban area of Boston [18], while the urban area of Phoenix (Arizona), also in the United States, was analysed with high-resolution Quickbird imagery [9]. MODIS LST data are the basis for the UHI study of twelve Indian cities with over 2.5 million inhabitants [19] and a study of 717 cities worldwide [20]. Landsat data are a standard resource in LST studies [21–28], owing to their high spatial coverage and resolution, free access and long time series [29]. Although there are limitations and uncertainties when deriving LSTs from Landsat imagery [30], it does allow data to be obtained every 30–120 m, a spatial resolution that cannot be achieved with weather observatories [1]. On the other hand, Landsat data are acquired every 16 days and are exclusively diurnal, which means that the nighttime intensity of UHIs is not captured [25]. This has led to strategies to estimate nighttime UHIs by drawing on satellite imagery, as well [13].

The intensity and spatial pattern of UHIs hinge on the characteristics of the land surface, which are heavily influenced by land use/land cover (LULC) [3,31]. Each LULC has a different effect on temperature, as they present unique optical spectrum, humidity, and temperature properties [32]. Thus, it makes sense to link remote sensing data with this spatial resolution to the various land covers [20,23,28,33,34]. The combination of Landsat satellite and CORINE Land Cover data has been used to obtain LST data and study UHIs, albeit with a limited number of images [24], as the authors had to process them to derive the LST.

While a large number of UHI studies have investigated cities in China, the United States, and Canada [10], there is no shortage of studies in Spain [4,17,24,27,35–47], where the UHI is equally significant, as the country's urban population stood at 82% in 2023, according to World Bank figures [48]. Spain is also one of the European countries with the greatest development of artificial cover [27,43]. Indeed, some references overlap with the one presented here in their study area, albeit with a different perspective, namely, weather stations and the Spanish Land Use and Land Cover Information System (SIOSE in Spanish) database [49].

This study, enabled by the Climate Engine platform, allows for a long time period, which is a prerequisite identified in LST studies with Landsat images [50]. This study's objectives were as follows:

- determine the variation in land cover and land use around the main urban areas between 1990 and 2018;
- determine the main flows between the two dates;
- derive monthly and annual temperatures for each land cover;
- calculate thermal trends;
- ascertain the monthly thermal behaviour of the main land covers.

The last three points allow us to achieve the primary objective of this study, the thermal behaviour of the different land covers.

2. Materials and Methods

2.1. Study Area

The study area was the main urban nuclei in the regions of Valencia and Murcia on the Spanish Mediterranean coast. These cities were the four provincial capitals, as follows: from north to south, Castellón, Valencia and Alicante in the Valencian Region and Murcia in the Region of Murcia, as well as Elche, the third-largest urban area in the Valencian Region (Figure 1), which we added.

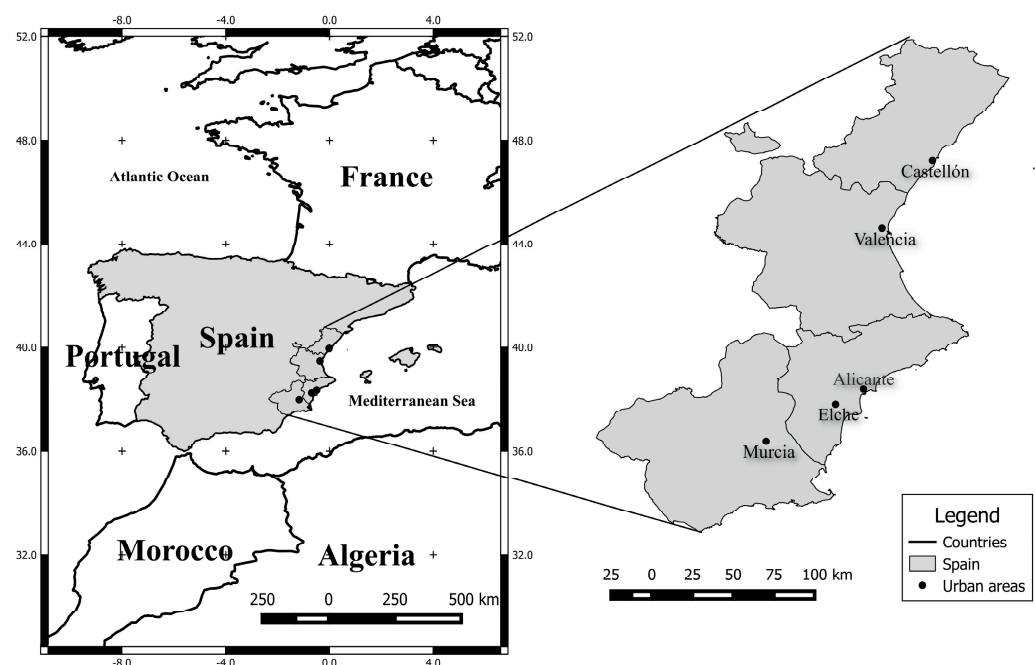


Figure 1. Location map of the urban areas surveyed.

The region has seen a significant increase in urban space, which has already been demonstrated in previous studies [51] using aerial photographs comparing the 1956 American flight by the Army Map Service of the United States Department of Defense [52] and the 2018 images from the National Plan of Aerial Orthophotography (PNOA in Spanish) available at the Geographic Information National Centre (CNIG in Spanish) [53]. The first advance in this new research consisted of going back a significant step in time by georeferencing the urban maps of the provincial capitals dated 1910 [54], which are also available electronically at the CNIG. This gives a fairly robust idea of the urban development of the main cities over the last hundred years (Figure 2).

In Spain, the smallest administrative division is the municipality, below the regions and provinces. Table 1 shows the official population data by municipality, even though urban areas in large cities stretch beyond these limits.

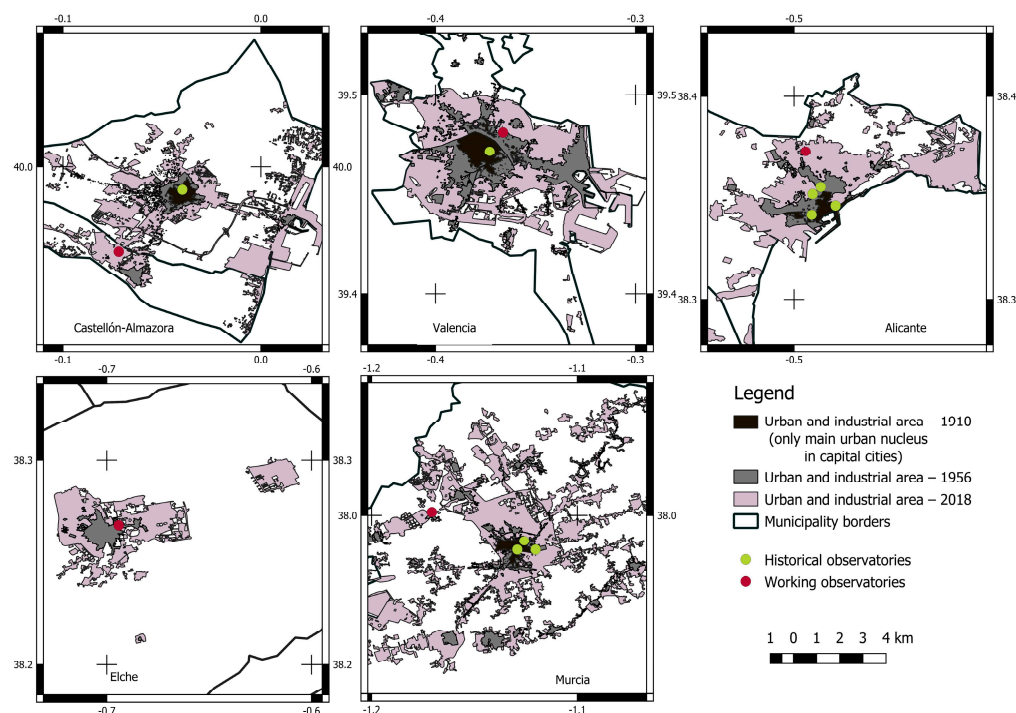


Figure 2. Growth of urban centres above 100,000 inhabitants and location of State Meteorological Agency (AEMET in Spanish) weather observatories. Source: [52–54].

Table 1. Municipal population and percentage of the provincial total (2023).

Municipalities	Population	% Provincial
Castellon	176,238	29.18
Valencia	807,693	30.41
Alicante	349,282	17.91
Elche	238,293	12.22
Murcia	469,177	30.22

Source: [55].

While municipal data can provide a rough estimate, this study went beyond these administrative boundaries. After a first test, taking municipal boundaries as a study framework was discarded given the sometimes fringe location of the official AEMET observatories within the administrative boundaries, as is the case of the Castellón–Almazora observatory (Figure 2), and the enormous disparity in size of the municipalities; from 142.7 km² in Castellón and Almazora and 136 km² in Valencia, the areas increase southwards, rising to 202 km² in Alicante and 325.5 km² in Elche before culminating in 885 km² in Murcia, one of the largest municipalities in Spain. The geographical context in which urban areas stretch across municipal boundaries prompted us to draw a polygon centred on operational urban observatories at a scale of 1:75,000, giving an area of about 417 km² for each urban area; this enabled us to quantify the artificial growth around the observatories while keeping a rural environment, thus enabling us to ascertain the impact of major land use changes on temperatures.

2.2. Materials

Two databases were harnessed in this study. Firstly, CORINE Land Cover, with its five available versions, 1990, 2000, 2006, 2012 and 2018. Coordination of Information on the Environment (CORINE) has become a flagship component of the European Environment Agency’s Copernicus Land Monitoring Service, providing essential information on European LULC for over three decades. The years 1990 [56] and 2018 [57] were used to observe

the start and end points of the series. This facilitated an analysis of changes in land use and land cover in recent decades in the surroundings of urban observatories.

CORINE classifies the terrain into various land covers with a degree of detail at three levels, from the most generic Level 1 to the most detailed Level 3. Level 1 has the following four categories: artificial surfaces, agricultural surfaces, forest and seminatural areas, and wetlands, which are expanded into 15 subcategories at Level 2 (Table 2) and 44 at Level 3 [58]. In this paper, Level 2 (intermediate level) was used to distinguish between urban and industrial areas while also keeping the number of categories to a minimum. The polygons of the different LULCs will be used for the extraction of LST and NDVI data.

Table 2. Level 1 and 2 categories and level codes in CORINE Land Cover.

Level 1	Level 2	Codes
Artificial surfaces	Urban fabric	11
Artificial surfaces	Industrial, commercial and transport units	12
Artificial surfaces	Mine, dump and construction sites	13
Artificial surfaces	Artificial, non-agricultural vegetated areas	14
Agricultural areas	Arable land	21
Agricultural areas	Permanent crops	22
Agricultural areas	Pastures	23
Agricultural areas	Heterogeneous agricultural areas	24
Forest and seminatural areas	Forests	31
Forest and seminatural areas	Scrub and/or herbaceous vegetation associations	32
Forest and seminatural areas	Open spaces with little or no vegetation	33
Wetlands	Inland wetlands	41
Wetlands	Maritime wetlands	42
Wetlands	Inland waters	51
Wetlands	Marine waters	52

Source: [58].

The figures for urban growth (Figure 2) were based on the images from the American flight series B (1945–1946) produced by the Army Map Service of the United States Department of Defense at a scale of 1:32,000 and frames from the 2018 PNOA flight. Both are available at the CNIG via Web Map Service (WMS) and through the CNIG download centre.

The other database used was the land surface temperatures (LSTs) and normalised difference vegetation index (NDVI) measured by the Landsat satellite constellation [59]. Although the series began in 1972 [22], Landsat 5, 7, 8, and 9 have completed a database of surface temperatures since 1984 with a resolution of 30–120 m, which is accessible as a result of the Climate Engine project [60,61]. This is one of several applications that have been built into Google Earth Engine (GEE) and can play a significant role in climate monitoring [62]. The reliability of the databases stored in the GEE is confirmed by the hundreds of articles that have used them [63–65]. Among the various applications, the Climate Engine Project stands out among those that monitor the climate [65,66]. Some papers have already made progress in using the Climate Engine and LULC to study UHIs [67–70]. To the best of the authors' knowledge based on the citation list of the reference article [60], this is one of the first UHI studies using the Climate Engine and LULC and a pioneer in cities in Europe and, therefore, in Spain. A study on several cities in Bulgaria was restricted to establishing the correlation between NDVI and LST [71].

2.3. Methods

At the National Centre for Geographic Information's download centre [72], CORINE data were retrieved in the form of two multipolygon layers, one for the Peninsula-Balearic Islands and the other for the Canary Islands. Once the Peninsula-Balearic Islands layer had been extracted, the data were read, analysed, and displayed using R 4.3.1 software packages through the Rstudio 2023.06.0 platform (Table 3).

Table 3. R software packages used in this study.

Package	Tasks
geodata 0.5-9	Administrative boundaries
sf 1.0-16	Spatial data processing
utils 4.3.1	Reading csv files
data.table 1.14.8	Linking CORINE layers with categories
dlookr 0.6.3	Outlier imputation
imputeTS 3.3	Missing data imputation
tidyverse 2.0.0	Data processing, results by areas and comparative tables 1990–2018
ggplot2 3.5.1	Graphic visualisation
grDevices 4.3.1	Saving graphs and maps

The first step was to download and read the files with the information from the CORINE Land Cover database stored with EPSG code 25830. EPSG is the initialism for the “European Petroleum Survey Group” [73], originally from the oil industry and nowadays used as a reference. EPSG 25,830 corresponds to the reference system ETRS89 projection UTM zone 30N. Files from both 1990 and 2018 were cropped with the administrative boundaries of the regions of Valencia and Murcia for better, faster handling. The administrative data were extracted with the R geodata package. Their reference system is geographic, WGS84 (EPSG 4326), so they were first transformed into the ETRS89/EPSG 25,830 of the CORINE Land Cover layers. A legend was also added with the levels of the CORINE Land Cover layers, and a colour palette was designed for the maps.

QGIS 3.28.8 Firenze software was used firstly to reference the 1910 urban maps and secondly to visualise the data and define the study area in each urban nucleus. These areas, one for each urban area in this study, were used to crop the CORINE Land Cover study areas. The next step, again with R, consisted of intersecting these 1990 and 2018 LULC areas. These are the layers of flows between the LULCs that obviously include polygons in which there have been changes and others in which the LULC has stayed the same. These layers were dissolved to join the sectors in the same flow. The area was then calculated. These layers were used in the flow graphs and are available as non-published material.

There were around a hundred flows between land use categories for each of the five urban areas, and the most significant ones with a surface area of over 4–4.5 km² were selected. This simplified the analysis by avoiding dozens of land use changes in a very small area. Other lesser flows were added to these main ones to complete the table of trends and the urban area as a whole, with the abovementioned polygons measuring some 145 km², which were smaller in area in the cases of Castellon, Valencia, and Alicante that included marine portions.

The next step, consisting of retrieving LST data from the Climate Engine website [61,74], was entirely manual and provided data from a point or an area. The LULC change layer for each urban area was saved in shapefile format with the polygons of each land use change. This is the format supported by the website. The intricacies of the boundaries prevented downloading the data for each polygon and the entire period of available years (1984–2023) in a single go. Up to five downloads per polygon (445 downloads in total) had to be made, which was a tedious yet necessary process. To prevent errors when selecting and assigning polygons, the process was performed following prior visualisation of the polygons in QGIS software. Data for 1984 have been eliminated since their records begin in the month of April.

Once the temperature data had been obtained, 1000 observations per urban area were randomly sampled to check that the data corresponded to the correct flows. This was followed by a twofold process consisting of locating the outliers and their imputation by means of the capping method. This method replaced the upper outliers with the 95th percentile value and the lower ones with the 5th percentile. Next, temporary reference files were created to locate the months with no Landsat images and, therefore, with no data

available. The missing data were replaced using the weight moving average method based on the two closest observations (Table 4).

Table 4. Number of outliers and missing data in the data for the urban areas.

Urban Area	Total Flows	Analysed Flows	Outliers	Missing Data	Observations
Castellon	79	16	21	208	29,013
Valencia	106	20	54	199	36,868
Alicante	86	18	38	186	34,880
Elche	96	20	66	215	39,525
Murcia	94	23	18	612	29,795

The final step was to analyse the LST data with the R tidyverse package to obtain monthly averages by year, LULC flow, and urban area, annual averages by LULC flow and urban area, and monthly averages by LULC flow and urban area. Using the same package, NDVI data for non-urban land covers were analysed to consider the influence of vegetation on UHI strength. NDVI data were obtained for the years 2017 and 2019, i.e., around the last CORINE Land Cover collection in 2018, to avoid having data from a single year and, at the same time, to reduce the effect of possible changes in land use.

3. Results

There is a difference of almost forty years between the first (1990) and the most recent publication of CORINE Land Cover data (2018). These four decades brought sweeping changes to this flat, coastal, and vibrant territory led by tourism [75] and a growing population [76]. First, these changes will be analysed before examining their impact on surface temperatures.

3.1. LULCs in 1990 and 2018 in Castellon

The urban area of Castellon is the most northerly of the areas analysed. It is a flat area, spreading out across the Mijares floodplain and delta and bounded by low mountainous zones. In administrative terms, to the north of the River Mijares, there is the municipality of Castellon, the provincial capital that housed the historical observatory until 1975 in a secondary school in the town centre, and the municipality of Almazora, where the observatory is still operating in the Mijares industrial area close to the river of the same name. To the south and by population, there is the urban area of Villarreal, whose industrial park is connected in the west to Onda and in the south to Alquerias, a route that is rounded off with Burriana, which covers the southern side of the Mijares delta.

Permanent crops, the typical orange trees of the Valencian Region, were the main cultivation in both 1990 and 2018. In 1990, at 244 km² they accounted for 76% of the surface area, a figure which, by 2018, had fallen to 189 km² or 58.9%. Heterogeneous agricultural areas also decreased from 23 km² to 13 km². The most striking increases are in two categories of artificial surfaces, namely, the urban fabric and the industrial, commercial, and transport units. Each gained some 21 km² to reach 40 km² and 29 km², 12.6% and 9%, respectively. The historical observatory located in the Francisco Ribalta Secondary School is in the provincial capital's city centre. Although records began in 1879, the first years have been lost, and they have only been preserved since 1911. Hence, it was always surrounded by an urban environment, which has steadily grown, as shown by the 1990 and 2018 maps (Figure 3). Indeed, an almost continuous urban-industrial environment has emerged running from the coastal strip of Castellon and Almazora through the capital and extending towards Villarreal, where it splits into two arcs to the west and south. This growth has surrounded the current Castellon–Almazora observatory, which was originally on a small industrial estate that is now much larger.

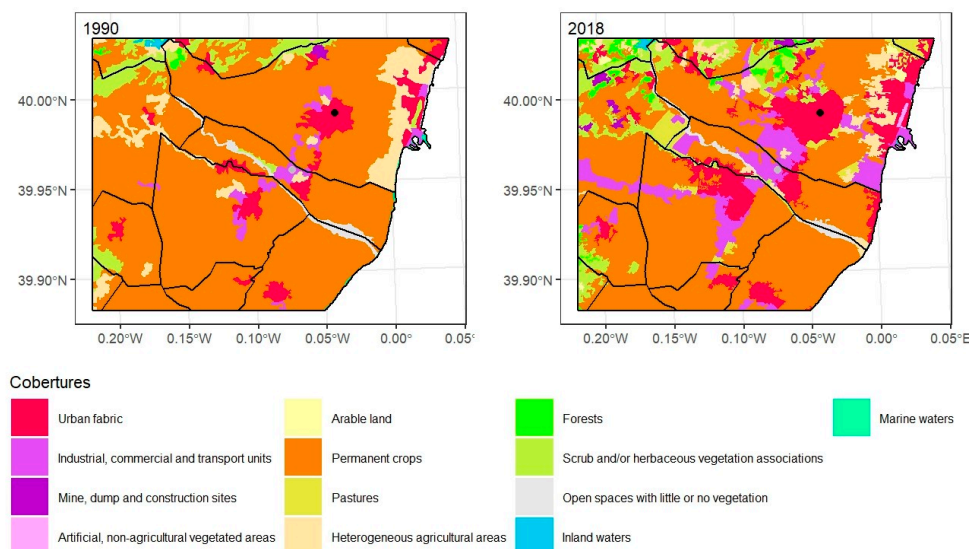


Figure 3. LULC distribution in Castellon's urban area between 1990 (**left**) and 2018 (**right**), with historical (black point) and working (grey point) observatories. Source: "Generated using European Union's Copernicus Land Monitoring Service information; <<https://doi.org/10.2909/5c1f2e03-fcba-47b1-afeb-bc05a47bada0>> <<https://doi.org/10.2909/71c95a07-e296-44fc-b22b-415f42acdfd0>>".

Permanent crops remained dominant, yet the artificial surfaces, both urban fabric and also industrial, commercial, and transport units (16 km² each), had grown at their expense in the urban-industrial continuum described above. The new urban areas wrested from permanent crops are equal to the urban fabric of 1990. Artificial surfaces have also taken territory from other agricultural areas and natural vegetation, albeit to a much lesser extent. This includes the almost 5 km² of urban fabric built in what used to be heterogeneous agricultural areas. The abandonment of orange groves is well-documented by their reversion to minor uses, such as pastures, heterogeneous agricultural areas, and scrub and/or herbaceous vegetation associations.

3.2. LULCs in 1990 and 2018 in Valencia

The urban area around the city of Valencia studied here is the main part of the regional capital, aside from the southern section, where l'Albufera Natural Park is located. The city of Valencia was initially on the southern bank of the River Turia, a few kilometres from the coast. However, urban growth over the course of the 20th century meant that the city reached the coastline (Figure 4). The weather observatory was set up in the University of Valencia's La Nau building in the original city location and operated between 1859 and 1937. The baton was taken up by the current observatory in the then-new urban areas to the north of the old Turia riverbed in Viveros Park, defined by the CORINE Land Cover base as an artificial, non-agricultural vegetated area.

Urban and industrial development spread in other directions following the main communication routes, as follows: to the west towards Madrid and to the south towards Alicante. In 1990, there were the following three main agricultural areas around Valencia: permanent crops, arable land, and heterogeneous agricultural areas. The urban counterpoint to the famous "Huerta de Valencia" market garden zone was 61 km² of urban fabric and 26 km² of industrial, commercial, and transport units. By 2018, these agricultural areas had lost 55 km², with the main beneficiaries being the artificial sectors, especially industrial, commercial, and transport units. In this year, artificial surfaces made up 48% of Valencia's urban environment, compared to 32% in 1990. The territorial transfers are more complex in Valencia since, as noted above, there were three agricultural areas in the "Huerta de Valencia", and all three helped to extend new urban, commercial, and industrial developments. Industrial, commercial, and transport units took more than 10 km² from permanent crops, almost 8 km² from arable land and just over 5 km² from heterogeneous

agricultural areas, a total of more than 23 km², which accounts for the 100% increase in their size. The urban fabric also grew at the expense of these agricultural areas, albeit to a lesser extent.

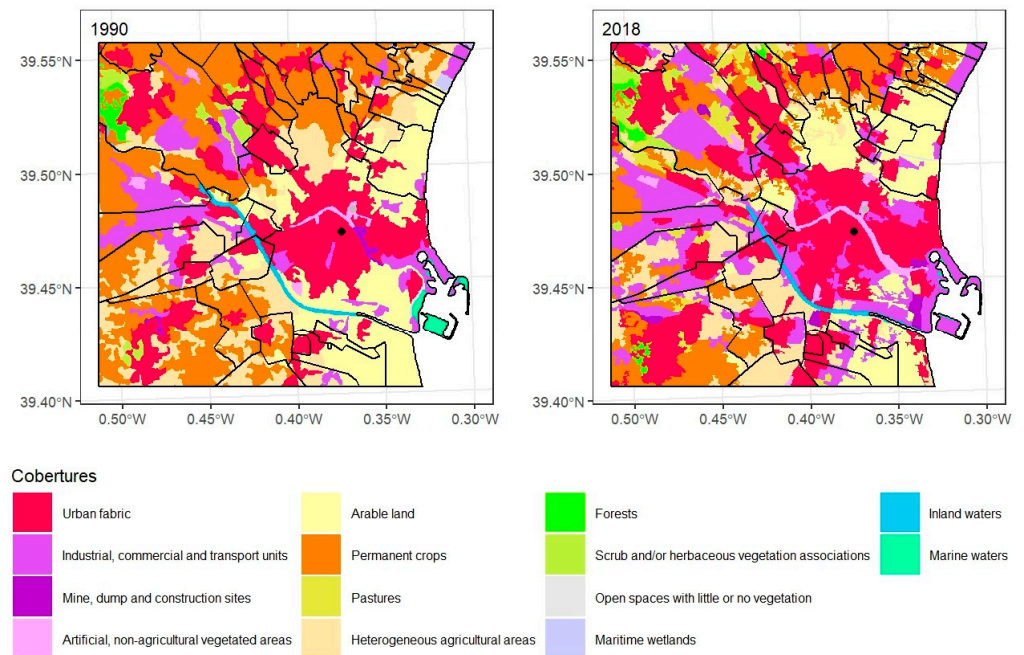


Figure 4. LULC distribution in Valencia's urban area between 1990 (left) and 2018 (right), with historical (black point) and working (grey point) observatories. Source: "Generated using European Union's Copernicus Land Monitoring Service information; <<https://doi.org/10.2909/5c1f2e03-fcba-47b1-afeb-bc05a47bada0>> <<https://doi.org/10.2909/71c95a07-e296-44fc-b22b-415f42acfd0>>".

3.3. LULCs in 1990 and 2018 in Alicante

Alicante is the most distinctive Valencian provincial capital in terms of its location, set in the arid lands of the south and on the coast. Its city hall is barely 190 m in a straight line across the famous Alicante Esplanade from the port, specifically from the plaque showing the 0 m reference level of Spanish cartography. Its closeness to the coast might be explained by the protective presence of two imposing castles, San Fernando and Santa Barbara. The plain they overlook has seen the expansion of the capital of Alicante and the successive allocation of its historical weather observatories, as follows: Asylum Garden (1855–1875), Former Provincial Secondary School (1876–1938), and Garden City, since 1938 and still in operation. As its name suggests, it is in a small area of discontinuous urban fabric barely 130 m from the northern edge of Alicante's urban fabric. Between 1933 and 1938, the Provincial Secondary School's observatory worked alongside another, which was first set up in the seismological centre and later, in the aforementioned San Fernando Castle.

The following two agricultural areas predominated around Alicante in 1990: permanent crops (53 km²), especially fruit trees, and heterogeneous agricultural areas (135 km²). Evidence of its location in the more arid southeast was the 54 km² taken up by scrub and/or herbaceous vegetation associations. Meanwhile, artificial surfaces had 33 km² in the urban fabric, namely, Alicante's urban nucleus with expansion to the northwest in the neighbouring municipality of San Vicente del Raspeig and towards the north in the population nuclei of Muchamiel and San Juan, plus the Alicante and El Campello coastal strip. The impact of tourism left its mark. The 9 km² of industrial estates were scattered across Alicante and San Vicente (Figure 5).

Almost 40 years later, artificial surfaces had grown significantly, especially in the north. They had practically overrun the municipality of San Vicente, to the extent that Alicante's neighbouring town experienced a similar expansion. The coastal strip had become an urban

continuum. Urban fabric stood at almost 70 km², 23.5% of the territory, while industrial, commercial and transport units covered just over 20 km² (Figure 5).

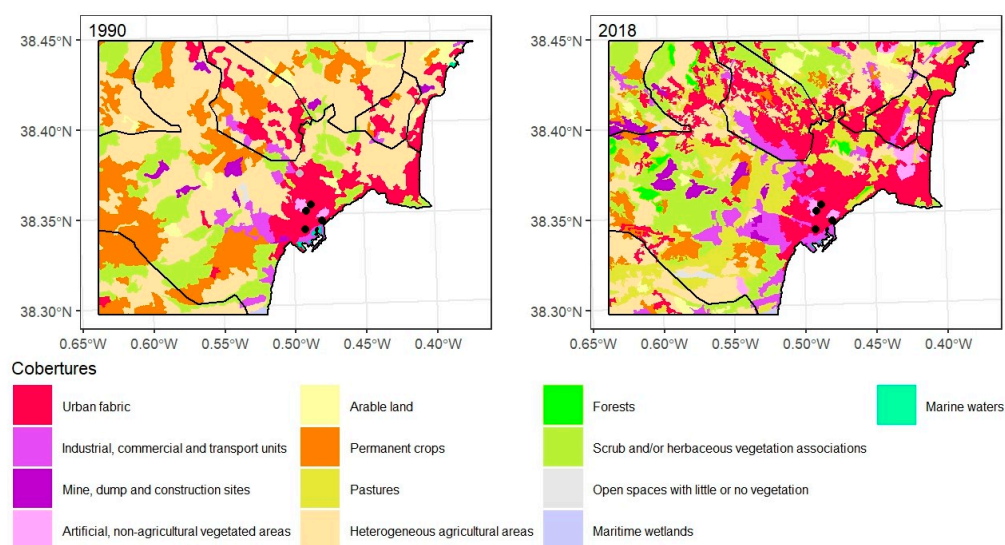


Figure 5. LULC distribution in Alicante's urban area between 1990 (left) and 2018 (right), with historical (black point) and working (grey point) observatories. Source: "Generated using European Union's Copernicus Land Monitoring Service information; <<https://doi.org/10.2909/5c1f2e03-fcba-47b1-afeb-bc05a47bada0>> <<https://doi.org/10.2909/71c95a07-e296-44fc-b22b-415f42acfd0>>".

The once predominant heterogeneous agricultural areas divided their land, especially into urban areas (27.2 km²), primary uses, such as pastures (25.9), and scrub and/or herbaceous vegetation associations (28.1). The urban fabric rounded off its growth at the expense of another agricultural cover, permanent crops. Industrial, commercial, and transport units increased by taking space away from heterogeneous agricultural areas, permanent crops, and scrub and/or herbaceous vegetation associations. There were significant territorial transfers between non-artificial surfaces. In addition to those mentioned above originating in heterogeneous agricultural areas, there was also the flow from scrub and/or herbaceous vegetation associations to pastures and from permanent crops, with heterogeneous agricultural areas finally as beneficiaries. There were other flows under 10 km² from heterogeneous agricultural areas to permanent crops or from permanent crops to pastures or scrub and/or herbaceous vegetation associations, reflecting the prevalent decline in agriculture on the Mediterranean coast in general [77] and in the province of Alicante in particular [78].

3.4. LULCs in 1990 and 2018 in Elche

The municipality of Elche, which is next to Alicante, lies on the same flat land deposited by the tertiary seas. Indeed, Alicante's El Altet airport, one of the busiest in Spain as it welcomes tourist flows to the sunny southeast [79], is in the municipality of Elche. It is here that one of the weather observatories still in operation is located. In this respect, Elche has no historical records prior to the beginning of the 20th century, yet it has three weather stations that began taking measurements around the middle of the last century, as follows: one of them in the city expansion area, on the left bank of the Segura River; another on the edge of the historic centre on the right bank; and a third, Elche-Campo Agrícola, which as its name suggests, is on land that was turned from a heterogeneous agricultural area into an industrial, commercial, and transport unit.

As was to be expected and just like in nearby Alicante, heterogeneous agricultural areas were dominant here in 1990 at 214 km², which is slightly over half of the territory. By 2018, however, they had shrunk to 111 km², meaning that by then, they only accounted for a quarter. This is still a striking figure for a single cover, yet it does speak to a sharp

decline. Next in line are scrub and/or herbaceous vegetation associations (86 km²) and two other agricultural areas, permanent crops and arable land. Interestingly, there are 15 km² of wetlands in the Santa Pola salines and El Hondo lagoons. In the late 20th century, the urban fabric of Elche, together with neighbouring parts of Santa Pola on the coast and Aspe and Crevillente inland, covered 21 km², while industrial, commercial, and transport units added almost 6 km² of artificial surfaces to the area (Figure 6).

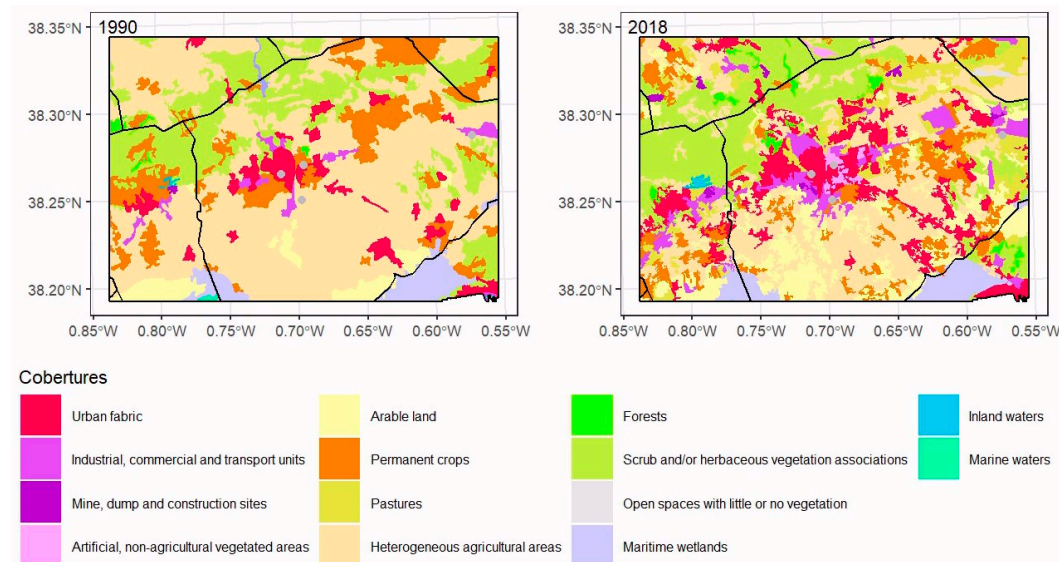


Figure 6. LULC distribution in Elche's urban area between 1990 (left) and 2018 (right), with historical (black point) and working (grey point) observatories. Source: "Generated using European Union's Copernicus Land Monitoring Service information; <<https://doi.org/10.2909/5c1f2e03-fcba-47b1-afeb-bc05a47bada0>> <<https://doi.org/10.2909/71c95a07-e296-44fc-b22b-415f42acfd0>>".

By 2018, the urban fabric had grown to almost 50 km², and the industrial and commercial part was over 20 km². The urban-industrial expansion follows a clear linear west-east trend alongside the communication routes between Murcia and Alicante. Growth is more urban towards the coastal and, therefore, tourist area of Santa Pola (Figure 6). This artificial growth took place to the detriment of permanent crops and heterogeneous agricultural areas since scrub and/or herbaceous associations were maintained, and arable land even increased.

3.5. LULCs in 1990 and 2018 in Murcia

Murcia extends the flat lands, where the communication routes run towards the eastern Andalusian coast. However, the city is far from the sea, dominating its fertile "huerta" (market garden area). A series of mountain ranges herald the Betic elevations to which they belong and, in fact, have the same characteristic southwest–northeast alignment. There have been many ups and downs in weather measurements. The first observatory was founded in 1856 in the very characteristic location of the Provincial Secondary School, and the measurements continued until 1954 when they were switched a little further north in the urban nucleus to the university campus. This observatory's life was extremely short, and in 1967, recordings began in the Vistabella neighbourhood. Although this observatory is still in operation, it is restricted to temperature and rainfall values, as in 2000, the main weather centre was relocated to the boundary of the Guadalupe district.

The overwhelming agricultural ascendancy in these flat lands on the shores of the Mediterranean is a constant, and Murcia is no exception. Permanent crops at 28.6% and heterogeneous agricultural areas at 38.1% account for two-thirds of this territory. They are made up of the northern part of the municipality of Murcia plus a small sector of Santomera in the northeastern corner together with, in the northwestern part and in an anticlockwise

direction, part of Molina de Segura and almost the entirety of the municipalities of Alguazas and Las Torres de Cotillas. The jigsaw is rounded off with Alcantarilla, wholly surrounded by Murcia. The agricultural landscape was completed by the meagre 17 km² of arable land, barely 4% of the area. A total of 49 km² was taken up by scrub and/or herbaceous associations, and 11 km² was open space with little or no vegetation, the highest figure in the five urban areas. These spaces with little or no vegetation stand in contrast to 16.6 km² of forests. Although the south is more arid, the Murcia area is the only one to host some mountainous terrain, specifically the Sierra de Carrascoy. The urban fabric covered an area of almost 35 km², especially the urban nucleus of the capital, and the distinct and numerous districts were lined up in the same direction as the plain. The picture was finished by 8 km² of industrial, commercial, and transport units, mainly in Alcantarilla and its neighbouring areas and along the road between Murcia and Molina de Segura (Figure 7).

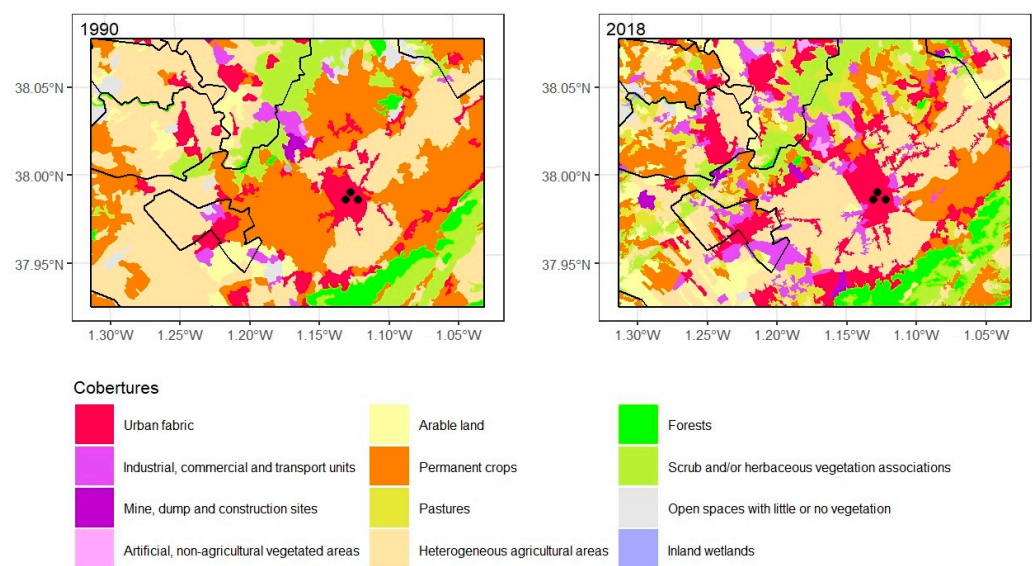


Figure 7. LULC distribution in Murcia's urban area between 1990 (**left**) and 2018 (**right**), with historical (black point) and working (grey point) observatories. Source: "Generated using European Union's Copernicus Land Monitoring Service information; <<https://doi.org/10.2909/5c1f2e03-fcba-47b1-afeb-bc05a47bada0>> <<https://doi.org/10.2909/71c95a07-e296-44fc-b22b-415f42acfd0>>".

These industrial areas had increased by 248%, occupying 28 km² in 2018. They had grown from less than 2% to almost 7% and mushroomed around most of the urban nuclei, forming a network to the northwest of the capital of Murcia. The urban fabric took up 60 km², gaining from heterogeneous agricultural areas, permanent crops, and scrub and/or herbaceous vegetation associations. Industrial, commercial, and transport units had also pushed back these agricultural areas. As in Valencia, the strong pressure exerted by the capital and its adjacent urban areas generated a conurbation that devoured and broke up its famous "Huerta" [80]. There were also transfers between agricultural uses, in particular, the decline of permanent crops giving way to heterogeneous agricultural areas, with the most prominent territorial flow being 43 km², which is very striking in the cartography. Alguazas experienced a completely opposite flow.

3.6. Landsat LSTs

In short, the surroundings of the large cities of the Valencian Region and Murcia, a prominent part of the prosperous Mediterranean arc, have seen an increase in artificial surfaces mainly at the expense of the decline in agriculture and, to a lesser extent, in abandoned land taken up by scrub and/or herbaceous vegetation associations or by open spaces with little or no vegetation. The process is typical of the Spanish Mediterranean basin [27]. Only arable land has increased. In Valencia and Alicante, the process has

resulted in their urban and industrial fabrics becoming the main land cover. In the other urban environments, one or another kind of agricultural use (permanent crops in Castellon, heterogeneous agricultural areas in Elche and Murcia) is still prevalent, although it is on the decline. Even so, only in the Valencia and Alicante areas do artificial surfaces outnumber agricultural ones (Table 5a,b).

Table 5. (a) Area in km² of main artificial uses by year and urban area. (b) Area in km² of main agricultural uses by year and urban area.

(a)							
Urban Area	Urban Fabric	Urban Fabric	Ind., Com., and Transp. ¹	Ind., Com., and Transp. ¹	Artificial Total		
	1990	2018	1990	2018	2018		
Castellon	18.9	40.4	7.7	29.0	69.4		
Valencia	61.6	80.3	26.2	52.5	132.8		
Alicante	33.4	67.8	8.5	20.8	88.6		
Elche	21.4	48.1	5.9	20.6	68.7		
Murcia	34.8	59.8	8.2	28.4	88.2		

(b)							
Urban Area	Arable Land	Arable Land	Perm. Crop ²	Perm. Crop ²	Het. Agr. ³	Het. Agr. ³	Agric. Total ⁴
	1990	2018	1990	2018	1990	2018	2018
Castellon	0.0	1.3	244	189.0	23.1	13.0	203.3
Valencia	45.1	38.4	81.2	42.3	45.6	35.8	116.5
Alicante	6.8	8.1	53.2	15.5	135.0	56.0	79.6
Elche	16.0	46.8	54.2	37.0	214.0	111.0	194.8
Murcia	17.0	32.8	120.0	69.2	160.0	122.0	224.0

¹ Industrial, commercial and transport units. ² Permanent crops. ³ Heterogeneous agricultural areas. ⁴ Agricultural. In green, increasing changes. In red, decreasing changes. In bold, the main land use by year and urban use in the two tables. In the case of the totals, the main artificial or agricultural use. "Generated using European Union's Copernicus Land Monitoring Service information; <<https://doi.org/10.2909/5c1f2e03-fcba-47b1-afeb-bc05a47bada0>> <<https://doi.org/10.2909/71c95a07-e296-44fc-b22b-415f42acfd0>>".

There are numerous LULCs and many territorial transfers between them. It should be noted that there are 15 Level 2 LULCs used and around one hundred combinations of these land covers between 1990 and 2018 for each urban area. To facilitate this analysis, we only took into consideration the most significant land covers in terms of area.

The changes in annual LST values by urban area show the characteristic phases of the global series with an early decline associated with the June 1991 eruption of the Pinatubo volcano in the Philippines [81], followed by a weak upturn in values in what has been termed the global warming hiatus [82]. These two phases can be seen in the series of all LULC changes. By contrast, there is the thermal downturn of 1996, which was barely perceptible in Murcia, the one in 2002, which was more prominent in the southern urban areas, the one in 2012, which was particularly pronounced in Murcia, and the one in 2021, which conversely, was found in the two northern observatories (Figure 8).

The different urban areas with their respective UHIs also coincide in the higher averages of the industrial, commercial, and transport units, whose values are especially striking in Castellon and Valencia. The Plana de Castellon presents an average temperature of its urban fabric, which is 1.1–1.6 °C higher than the surrounding agricultural fields, values that rise in the case of the industrial, commercial, and transport units to 3.7–4.3 °C. The UHI is smaller in the other urban areas. Indeed, in the case of Alicante, urban fabrics have lower temperatures. Its location, which is unique among the urban areas studied, as it is open to the sea, might have an influence due to local sea breezes (Figure 8 and Table 6).

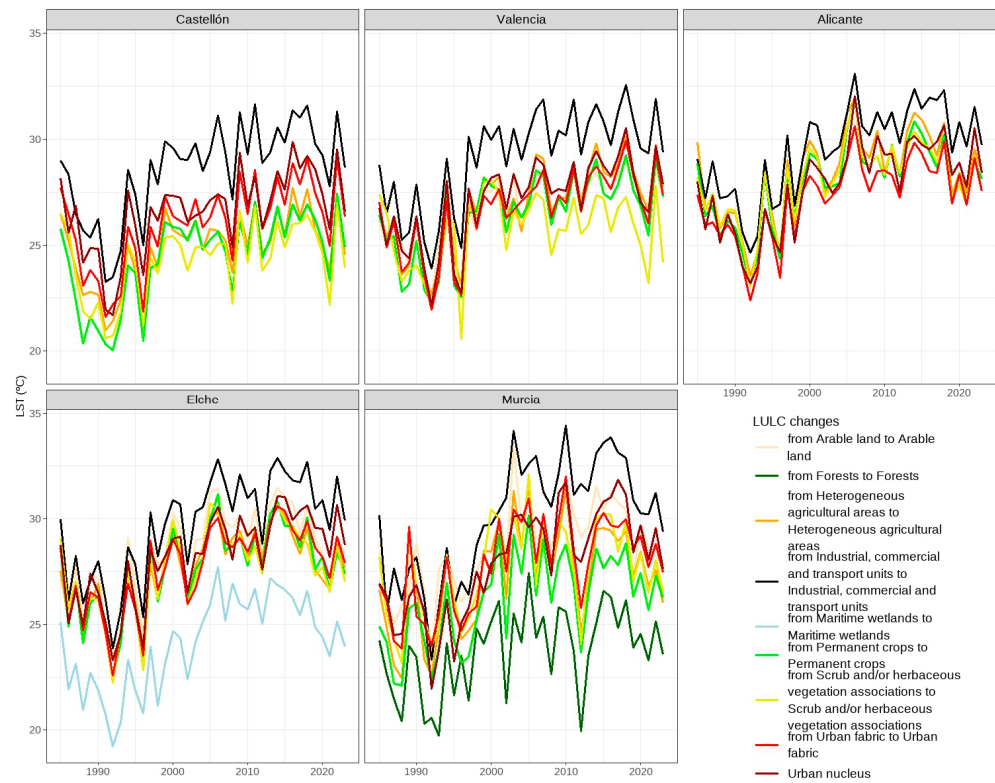


Figure 8. Annual evolution of LST by urban area for constant uses. Source: [60,61,74]. “Generated using European Union’s Copernicus Land Monitoring Service information; <<https://doi.org/10.2909/5c1f2e03-fcba-47b1-afeb-bc05a47bada0>> <<https://doi.org/10.2909/71c95a07-e296-44fc-b22b-415f42acdfd0>>”.

Table 6. Average LST (°C/year) in the most significant unchanged LULC flows.

Urban Area	Urb. Urb. ¹	Ind. Ind. ²	Pcrop. Pcrop. ³	Hga. Hga. ⁴	Scrub. Scrub. ⁵	Urban Nucleus
Castellon	26.4	29.1	24.9	25.2	24.6	27.1
Valencia	27.1	29.7	26.9	27.5	26.0	27.6
Alicante	27.7	30.0	28.3	28.7	28.3	28.3
Elche	28.1	30.2	28.0	28.0	27.9	28.7
Murcia	28.3	30.5	26.6	27.6	28.0	28.4

¹ From urban fabric to urban fabric. ² From industrial, commercial and transport units to industrial, commercial, and transport units. ³ From permanent crops to permanent crops. ⁴ From heterogeneous agricultural areas to heterogeneous agricultural areas. ⁵ From scrub and/or herbaceous vegetation associations to scrub and/or herbaceous vegetation associations.

The low urban values have prompted a more detailed study of the reasons, targeting the urban structure. The urban fabric cover is at Level 2 accuracy, but when going down to the more detailed Level 3, the CORINE Land Cover separates continuous urban fabric and discontinuous urban fabric. When extracting data for urban fabrics, this factor that lowers their averages is not taken into account. To confirm this, LST points were extracted in the urban fabrics of Valencia and two towns on its outskirts, Godella and Torrent, which are continuous urban fabrics, and they were compared with discontinuous urban fabrics in their vicinity. The temperatures of these discontinuous fabrics were 25.7 °C, compared to 27.7 °C in Godella, 27.9 °C in Valencia, and as high as 28.3 °C in Torrent.

Hence, LST averages were calculated for the urban nuclei of the five main cities under study. As expected, these urban nuclei reveal differences with respect to their adjacent agricultural and vegetation areas. As noted above, the contrasts are very sharp in Castellon and smaller in the case of Alicante. In Valencia, they are +0.5 °C in the case of permanent crops and practically non-existent for scrub and/or herbaceous vegetation associations,

which, on the other hand, are very scarce in the Valencian urban area. In Elche, they are $+0.7\text{--}0.8\text{ }^{\circ}\text{C}$, which is very close to the margin of non-artificial use, whereas in Murcia, permanent crops are $1.8\text{ }^{\circ}\text{C}$ lower in their LST, 0.8 in heterogeneous agricultural areas, and 0.4 in the plentiful scrub and/or herbaceous vegetation associations (Table 6).

The differences vary around this average both annually (Figure 8) and monthly (Figure 9). They tend to be smaller in the winter months, gradually widening to reach their peak in warmer months. Landsat images are diurnal and thus reflect UHI characteristics during the hottest hours of the day. This evolutionary pattern is quite patent in Castellón, while in Valencia, it is blurred by the behaviour of permanent crops. In Alicante, agricultural areas are warmer than the urban nucleus. The capital of Alicante already had the softening effect of its proximity to the sea, but this is reflected even more in the warmer months when the sea breezes are stronger. In Elche, the greatest differences are from April to June, and in the hottest months, arable land is warmer than urban fabrics. This is also true in nearby Murcia, which most likely explains the special features of this use in areas that are more southerly and, at the same time, more arid.

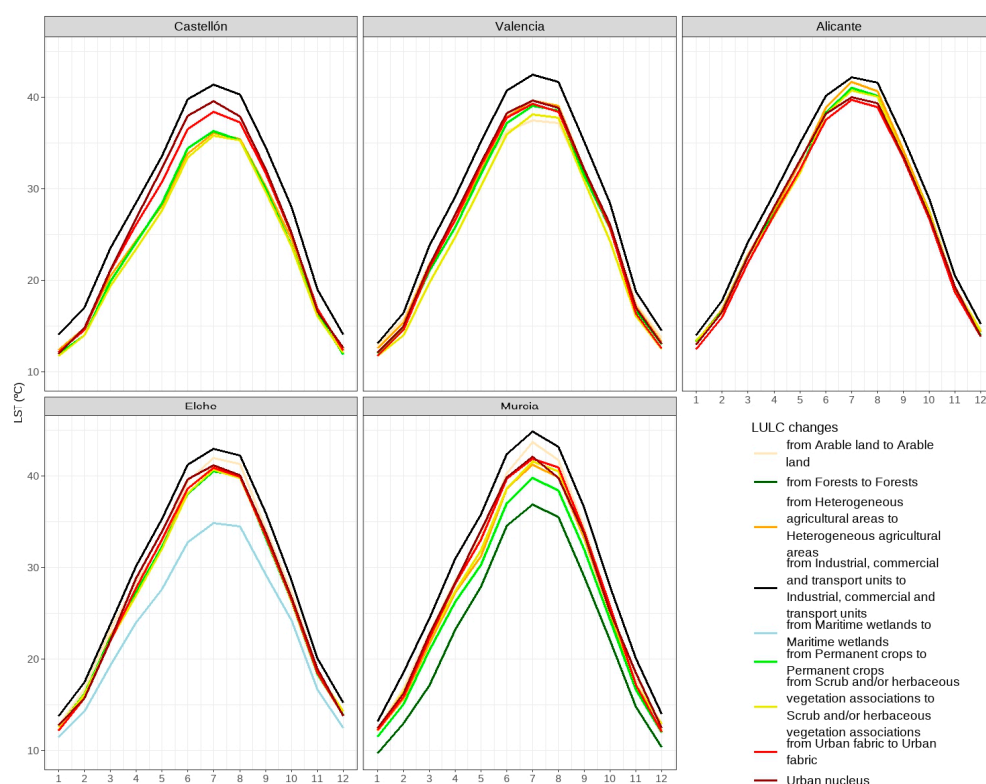


Figure 9. Monthly evolution of LST by urban area for constant uses. Source: [60,61,74]. “Generated using European Union’s Copernicus Land Monitoring Service information; <<https://doi.org/10.2909/5c1f2e03-fcba-47b1-afeb-bc05a47bada0>> <<https://doi.org/10.2909/71c95a07-e296-44fc-b22b-415f42acfd0>>”.

The thermal evolution of the urban areas of Elche and Murcia includes some exclusive LULCs, providing complementary information on the behaviour of the UHI. In the case of Elche, there are marine wetlands, the Santa Pola salines, and the El Hondo lagoons, while Murcia has the Sierra de Carrascoy forests. Although coastal lagoons are a typical formation in the Mediterranean arc, i.e., a low coastline where the sea swell has spread the materials deposited by torrential watercourses, these lagoons have not always been preserved. Consequently, they are only found in the Elche study area. The most significant of these lagoons, L’Albufera in Valencia, lies outside the city’s urban area. As for forests, they are usually preserved in mountainous areas, where sloping terrain hinders human settlement.

The conservation of these wooded areas against residential and tourist encroachment has been helped by their declaration as protected areas, and often, natural parks.

Elche's wetlands show much lower thermal values than those of the rest of the land covers. Their average temperature of 24.5 °C is far below the 28 °C of the agricultural land covers, the 28.7 °C of the urban nucleus, and, of course, the over 30 °C of the industrial, commercial, and transport units. Similar circumstances can be observed in Murcia's forests, whose average is even lower at 24.1 °C (Figures 8 and 9), which is a good example of the role that wooded areas can play in softening the UHI effect.

As a summary of the results for the different urban areas, Figure 10 shows the monthly evolution of the UHI, expressed as the difference in LST between the two artificial uses, the urban fabric and the industrial, commercial, and transport units, and three representative non-urban uses. The greater power of the UHI is detected in the warm months, which was already intuited in the monthly evolution of the LST shown in Figure 9. However, there is no lack of interesting differences. Castellon shows a single peak centred in June, while the remaining urban areas reflect a double peak in May and September, separated by relatively lower values. This behaviour is especially marked in Alicante, where the UHI in relation to the urban fabric is negative in practically all months and, in July and August, is lower than in winter. This inversion of the UHI is repeated in Elche, but very limited in months and intensity.

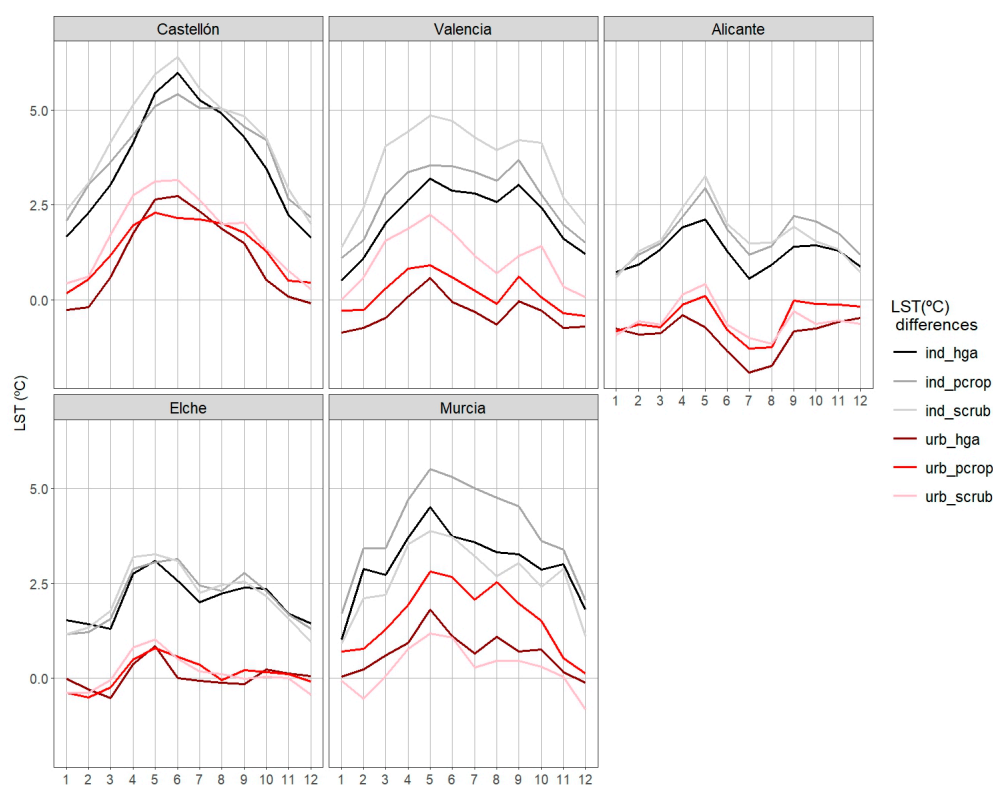


Figure 10. Monthly evolution of UHIs by urban area for constant uses. Ind_hga: industrial, commercial, and transport units minus heterogeneous agricultural areas. Ind_pcrop: industrial, commercial, and transport units minus permanent crops. Ind_scrub: industrial, commercial, and transport units minus scrub and/or herbaceous vegetation associations. Urb_hga: urban fabric minus heterogeneous agricultural areas. Urb_pcrop: urban fabric minus permanent crops. Urb_scrub: urban fabric minus scrub and/or herbaceous vegetation associations. Source: [60,61,70]. "Generated using European Union's Copernicus Land Monitoring Service information; <<https://doi.org/10.2909/5c1f2e03-fcba-47b1-afeb-bc05a47bada0>> <<https://doi.org/10.2909/71c95a07-e296-44fc-b22b-415f42acdf0>>".

There are two key factors in the behaviour of the UHIs in the five urban areas, as follows: latitude, which influences precipitation and vegetation, and distance from the

coast, which determines the intensity of the breezes. As shown in Table 7, the average UHI decreases with latitude. Aridity increases towards the south, as clearly demonstrated by the lower vegetation indices. The city with the lowest UHI is Alicante, where low vegetation indices and a coastal location combine with strong summer breezes, the latter of which are responsible for the marked decrease in the UHI in summer. The moderating effect of the breezes is evident when comparing Alicante and Elche, urban areas with similar vegetation indices, but with differences in the UHIs, which is more intense in Elche, which is further from the coast. Murcia, the most inland of the urban areas, has an intense UHI, which is the second-most notable. The distance from the sea and the higher density of their agricultural crops and the resulting shadows stand out.

Table 7. NDVI values in the most significant non-urban LULCs and average UHIs.

Urban Area	Hga. ¹	Pcrop. ²	Scrub. ³	UHI (°C)
Castellon	0.434	0.484	0.451	2.69
Valencia	0.311	0.390	0.416	1.56
Alicante	0.270	0.291	0.231	0.42
Elche	0.274	0.310	0.246	1.11
Murcia	0.334	0.368	0.263	2.02

¹ Heterogeneous agricultural areas. ² Permanent crops. ³ Scrub and/or herbaceous vegetation associations. Source: [60,61,70]. "Generated using European Union's Copernicus Land Monitoring Service information; <<https://doi.org/10.2909/5c1f2e03-fcba-47b1-afeb-bc05a47bada0>> <<https://doi.org/10.2909/71c95a07-e296-44fc-b22b-415f42acfd0>>".

The seasonality of the UHI does not appear to be influenced by changes in vegetation, the index of which reflects a very similar monthly evolution in all urban areas (Figure 11); it peaks in spring and autumn and decreases in winter and summer, achieving the distribution of rainfall in the Spanish Mediterranean.

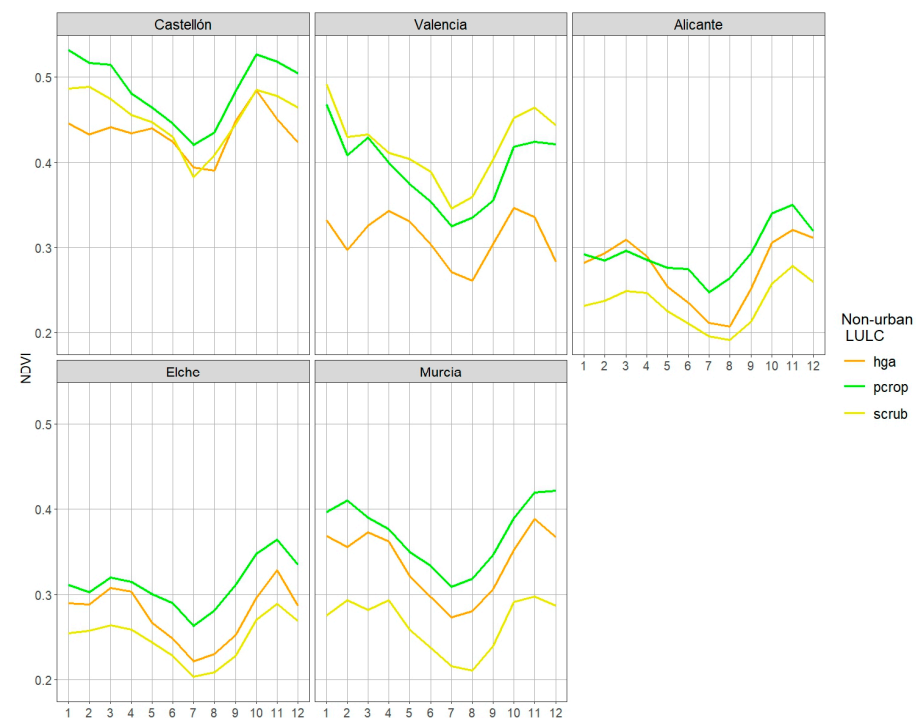


Figure 11. Monthly evolution of NDVI by urban area for the most important non-urban uses. hga: heterogeneous agricultural areas. pcrop: permanent crops. scrub: scrub and/or herbaceous vegetation associations. Source: [60,61,70]. "Generated using European Union's Copernicus Land Monitoring Service information; <<https://doi.org/10.2909/5c1f2e03-fcba-47b1-afeb-bc05a47bada0>> <<https://doi.org/10.2909/71c95a07-e296-44fc-b22b-415f42acfd0>>".

As with the thermal averages, the trends are particularly high for industrial, commercial, and transport units, especially with the conversion of agricultural land into this kind of artificial unit. The trends diminish when the conversion is in urban or agricultural land cover. For example, the change in heterogeneous agricultural areas is always below 0.1 °C/year (Table 8).

Table 8. LST trends (°C/year) in the most significant LULC flows.

Urban Area	Urb. Urb. ¹	Pcrop. Urb. ²	Ind. Ind. ³	Pcrop. Ind. ⁴	Pcrop. Pcrop. ⁵	Hga. Hga. ⁶	Hga. Pcrop. ⁷
Castellon	0.104	0.127	0.125	0.184	0.115	0.078	0.082
Valencia	0.112	0.109	0.138	0.137	0.111	0.116	0.099
Alicante	0.106	0.099	0.129	0.123	0.096	0.097	0.068
Elche	0.110	0.106	0.146	0.152	0.105	0.101	0.094
Murcia	0.111	0.127	0.168	0.127	0.107	0.108	0.082

¹ From urban fabric to urban fabric. ² From permanent crops to urban fabric. ³ From industrial, commercial, and transport units to industrial, commercial, and transport units. ⁴ From permanent crops to industrial, commercial, and transport units. ⁵ From permanent crops to permanent crops. ⁶ From heterogeneous agricultural areas to heterogeneous agricultural areas. ⁷ From heterogeneous agricultural areas to permanent crops. Source: [60,61,74]. "Generated using European Union's Copernicus Land Monitoring Service information; <<https://doi.org/10.2909/5c1f2e03-fcba-47b1-afeb-bc05a47bada0>> <<https://doi.org/10.2909/71c95a07-e296-44fc-b22b-415f42acdfd0>>".

The trends are high and shaped by a colder period at the beginning. The recovery of values after the fall due to the volcanic veil of 1991 leaves a very flat trend line, which has even included some negative trends since 2000. Most of these are trends in agricultural or shrub/herbaceous land cover (Figure 12).

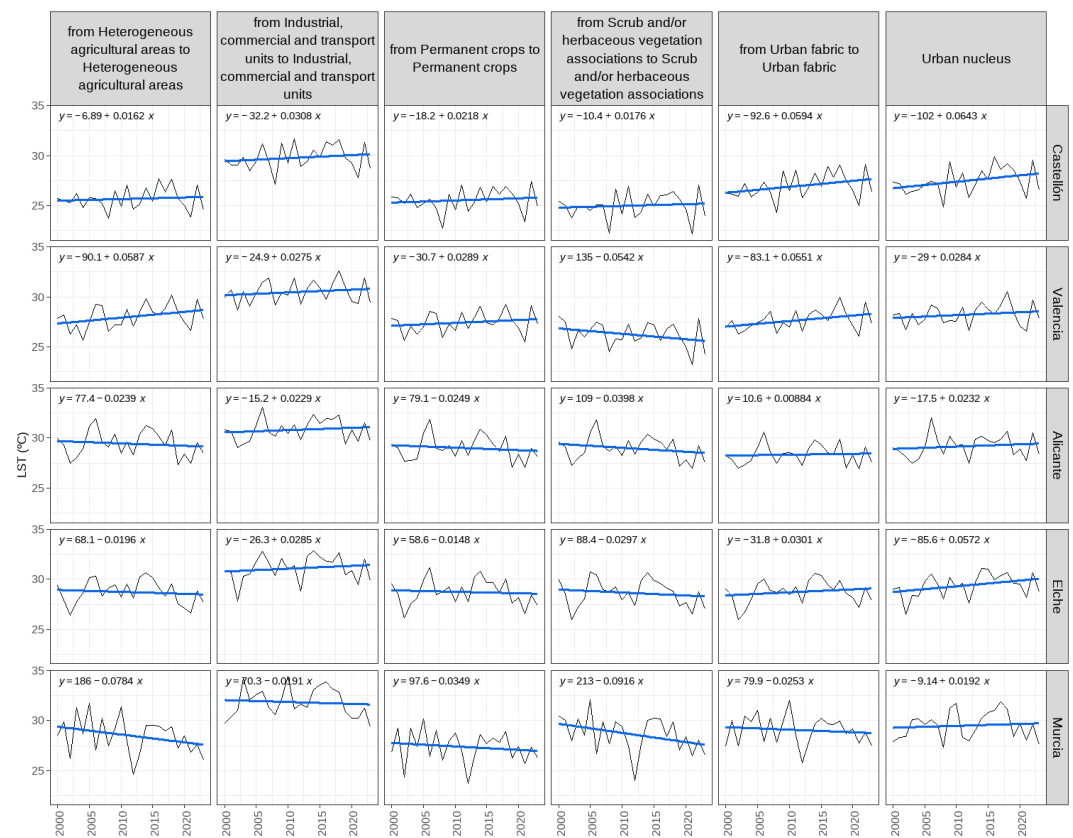


Figure 12. LST evolution (°C), in black lines, and trends (°C/year), in blue lines, since 2000 by urban area for constant uses. Source: [60,61,74]. "Generated using European Union's Copernicus Land Monitoring Service information; <<https://doi.org/10.2909/5c1f2e03-fcba-47b1-afeb-bc05a47bada0>> <<https://doi.org/10.2909/71c95a07-e296-44fc-b22b-415f42acdfd0>>".

4. Discussion

LST values are always higher than air temperature values and are more variable [83]. The main factor in LST varies over the course of the day; vegetation is the most prominent during daylight hours, and paving is the most prominent at night [83]. Other studies summarise it in the percentage of paved area [9] since an increase in this value will reduce the percentage of vegetated area. The higher LST values and trends in industrial, commercial, and transport units with little or no vegetation are extremely clear evidence in all the urban areas analysed. The results match those obtained at the seasonal level by also applying Landsat and CORINE Land Cover in the city of Barcelona [24], 300 kilometres north of our study area. Nonetheless, they are not so clear in urban fabrics, especially if the distinction between continuous and discontinuous fabrics is disregarded. The aforementioned study notes a greater difference in urban fabrics, which may be down to the fact that it does not take into account agricultural uses but does consider covers that are more differentiated in their behaviour in relation to urban impervious covers, such as green urban areas and forests.

As discussed above, Landsat LST data only capture diurnal data, so vegetation is a key factor in the thermal behaviour of the different LULCs and the characteristics of the UHI. Effectively, the results of our study reflect the importance of vegetation indices in explaining the magnitude of UHIs. Those urban areas with more vegetated agricultural areas show more intense UHIs. The greater vegetation differences between agricultural and natural areas and industrial, commercial, and transport units result in a large thermal contrast between these land covers. Urban areas have more densely populated zones, more industrial, commercial, and transport units, and more traffic, owing to their greater activity [11,13], and our results show that they make the greatest LULC contribution to UHIs.

The vegetation cover would explain the thermal distinctiveness of arable land, which is only vegetated for part of the year, always with more discreet plant growth and with high temperature averages, which, as noted above, can be higher than those found in urban nuclei.

There is no shortage of Landsat studies in which dry agriculture generates the highest LSTs [23,33]. Mediterranean natural and agricultural landscapes around cities in the summer are covered by a mixture of scattered trees, dry grasses, and bare soil that has already warmed up by the time the Landsat goes by [28] since their heat conduction capacity is low and they heat up quickly [40,42,43]. The intensity of the UHIs in the urban areas of our study decreases with latitude, which indicates less vegetation and less shade. Meanwhile, urban areas create shade with their buildings, which prevents warming [43].

The following two uses have demonstrated their importance in mitigating the effects of the UHI. Numerous studies point to the lower LST in urban vegetation areas. Although this is not so well documented here, it is an effect shown in the Murcian Sierra de Carrascoy forests, making increased green areas the most significant resource for reducing UHIs [40]. Urban fabrics with a greater vegetation presence will diminish the rise in LST [1], and this also explains why LST is lower in discontinuous fabrics, which are more vegetated than continuous ones. This is because the percentage of impervious surfaces is the main factor in LST [83]. The scale factor is further complicated by the fact that continuous urban fabrics include compact structures, typical of historic centres, which are more energy-efficient than less dense models found in more recent urban extensions [30]. Mediterranean cities, such as the ones in our study, have a very dense urban structure [84].

As for the water bodies in Elche's urban environment, they have low LST values, which can be accounted for by their large specific heat capacity and high water evaporation, which enable the regulation of atmospheric humidity and temperature [21]. Likewise, the weakness of Alicante's thermal values might be attributed to its closeness to the coast, and thus to a water body, and the greater intensity of the breeze system [28]. Barcelona, a city that is also located next to the sea, has shown a mitigation of UHI intensity in the summer months when breezes are strongest [35]. In Sydney, the summer temperatures

in the inland western suburbs are higher than those in the coastal eastern suburbs, with fluctuation related to the cooling effect of sea breeze [85]. While city size is a consideration, cities can be affected by the presence of water bodies and prevailing winds [11], and these local aspects are thought to be more influential than the city's size [86]. Once a threshold is crossed, wind can eventually eliminate the UHI [39,41,42]. This is reflected in the case of Alicante, with the least intense UHI, and by the opposite effect, in Murcia, the most inland of the urban areas. The seasonal magnitude of the UHI is also altered by the effect of sea breezes, shifting its maximum peaks to spring and late summer.

Equally, there is no shortage of contradictory conclusions explained by the scale effect [7] and the many factors shaping LST in a space as heterogeneous as the urban area and its surroundings [1]. Harnessing Landsat data from diurnal imagery hinders capturing the much higher and easier to characterise [13] UHI intensity at night [25]. Studies in the city of Phoenix (Arizona) with high-resolution Quickbird imagery concur with these results [9], yet conversely, a study with GOES satellite data on the urban environment of Boston found the highest surface UHI intensity in the middle hours of the day due to the lower thermal inertia of its artificial areas [18]. A large city such as Boston falls into the category of cities with high population density and a large cluster of human activities that experience more intense UHIs during daytime hours [86]. The daytime UHIs in the studied sector of the Spanish Mediterranean is higher in summer since the impact of the lower presence of vegetation is greater at this time of year [83]. Other Landsat studies reflect the highest intensity in the spring and summer months [23,24]. However, at the daily level, the studies reveal a great diversity of results on a seasonal scale due to the significance of local factors. Even in the Mediterranean area of our research, cities such as Athens and Parma have the highest UHIs during the day [12], while in Thessaloniki [87], Salamanca [39], Málaga [42], Zaragoza [37], or Santiago de Chile [88], it is at night. Madrid, Rome, Athens, Santiago de Chile [88], and Perth [89] have a higher urban impact in summer, whereas the highest intensity is observed in winter in cities such as Lisbon [86], Zaragoza [37], Málaga [42], Barcelona [17,35], and Casablanca [90].

This research and other studies mentioned in the references leave some issues open for the future, as follows: using nighttime images [13] for learning about nighttime UHIs at high spatial resolution; obtaining daily LST data to ascertain the effect of meteorological factors such as wind [11,38], which are judged to be more important than those related to the shape or size of the urban area [91]; acquiring data from weather stations whose locations could be improved by these results; drawing on NDVI data as a proxy for the percentage of urban green areas [25]; and using LULCs with more detailed resolution to understand the thermal behaviour of different urban structures and green or agricultural areas within the city borders. It is essential to improve knowledge of the heat island, a phenomenon with wide-ranging repercussions on human health [92], and knowledge that already provides important lines of action to follow in mitigating the effects of high temperatures. Some of these have already been suggested based on the results of this research, such as green areas, bodies of water, urban shaded areas, or the reduction of impermeable surfaces, among others. Recent studies with innovative proposals confirm this statement [93].

5. Conclusions

Prompted by the robust urban growth of the main cities on Spain's eastern coast, the main study's objective was to determine the thermal behaviour of the LULCs in the different urban areas, which is concredited in some objectives and already established in the final part of the introduction. These are our conclusions of these objectives.

Firstly, the analysis of the CORINE Land Cover LULCs led to the expected conclusion of substantial growth in artificial surfaces, especially in the urban areas of Valencia and Alicante, where these artificial surfaces are now predominant.

The second point, which is closely tied to the first one, is that this artificial growth took place at the expense of agricultural land and the few natural covers, usually scrub

and/or herbaceous vegetation associations, that remained in this fertile territory of high economic development and prolonged and intense settlement.

Once the LST series had been obtained for each polygon indicative of a change between LULCs, the next two objectives, the annual and monthly LST averages, were worked out, which, in turn, enabled us to interpret the thermal behaviour of the various covers. The results were shaped by the flyover of the Landsat satellites in the middle hours of the day.

The highest average values are found, with significant differences compared to agricultural peri-urban areas, in industrial, commercial, and transport units that are devoid of vegetation, which is the main factor affecting LST during daylight hours. They are therefore the main UHI driver. The results for urban fabrics are more diverse, reflecting the complexity of a cover that includes continuous and discontinuous urban fabrics. In the former, it is even possible to differentiate between historic centres with narrow streets and more recent urban developments in the form of city expansions. The thermal behaviour differs, and the results are extremely complex.

The differences are therefore greater between urban nuclei and agricultural areas, particularly in the case of permanent crops and not so much for scrub and/or herbaceous vegetation associations. Unlike urban areas, this cover and open spaces with little or no vegetation generate hardly any shade at the beginning of the daylight hours, which may explain the slight thermal differences. The arable land in Elche and Murcia, which is only vegetated for part of the year and smaller in growth, shares the same behaviour. Alicante is unique, with non-artificial areas featuring averages equal to or higher than those of urban areas, a trait explained by its coastal location and consequent strong breezes, especially in summer. The lowest thermal values are in wetlands and forests, which are only to be found in Elche and Murcia, respectively.

The intensity of the UHI decreases with latitude, which determines a decrease in rainfall and an increase in aridity. Non-urban uses, except for Murcia, show lower vegetation values that generate less shade and increase the LST, which can be close to the values of urban fabrics. The coastal location, especially in the case of Alicante, increases summer breezes and decreases the UHI, even eliminating it. Murcia, which is further inland, is the opposite case.

As for the trends, they present very high values influenced by the thermal drop at the beginning of the study period brought about by the eruption of the Pinatubo volcano in June 1991. As in the case of LSTs, the highest values are for industrial, commercial, and transport units. Recalculated from 2000 onwards, the trends are fairly flat and, in some cases, even downward.

These are the main conclusions of this study, which seeks to shed light on the complex issue of the UHI in terms of methodology and results. As noted above, further studies will of course be needed to gain greater insight into nighttime UHIs, LULCs with more spatial resolution, the effect of meteorological factors, or the use of meteorological data to support satellite imagery.

Author Contributions: All the authors, including E.M.C. and J.Q.S., have contributed to the design of the methodology and implementation of this research. They also helped in obtaining the Landsat temperature data. E.M.C. performed the data processing and the graphical and cartographic visualisation of the results with QGIS, and R. E.M.C. wrote the first draft. J.Q.S. took part in the review of this first draft and the writing and editing of subsequent drafts. All authors have read and agreed to the published version of the manuscript.

Funding: This research received no external funding.

Data Availability Statement: The original data used in the study are openly available at the websites included in references [52–58,61]. These data were analysed, summarized and presented by the authors. The final datasets are available on request from the corresponding author due to the great number of files.

Acknowledgments: The authors would like to acknowledge and recognise the great contribution that the Climate Engine website represents, which is made possible by the public availability of Landsat im-

ages. At the same time, they recognise the work of creating, maintaining, and improving opensource software, such as QGIS and R. “This publication has been prepared using the European Union’s Copernicus Land Monitoring Service information; <<https://doi.org/10.2909/5c1f2e03-fcba-47b1-afeb-bc05a47bada0>> <<https://doi.org/10.2909/71c95a07-e296-44fc-b22b-415f42acfd0>>”. “Generated using European Union’s Copernicus Land Monitoring Service information; <<https://doi.org/10.2909/5c1f2e03-fcba-47b1-afeb-bc05a47bada0>> <<https://doi.org/10.2909/71c95a07-e296-44fc-b22b-415f42acfd0>>”.

Conflicts of Interest: The authors declare no conflicts of interest.

References

- Peng, J.; Jia, J.; Liu, Y.; Li, H.; Wu, J. Seasonal Contrast of the Dominant Factors for Spatial Distribution of Land Surface Temperature in Urban Areas. *Remote Sens. Environ.* **2018**, *215*, 255–267. [[CrossRef](#)]
- World Bank Group. Urban Development. Available online: <https://www.worldbank.org/en/topic/urbandevelopment/overview> (accessed on 18 June 2024).
- Li, X.; Zhou, W.; Ouyang, Z.; Xu, W.; Zheng, H. Spatial Pattern of Greenspace Affects Land Surface Temperature: Evidence from the Heavily Urbanized Beijing Metropolitan Area, China. *Landsc. Ecol.* **2012**, *27*, 887–898. [[CrossRef](#)]
- Hidalgo-García, D.; Arco-Díaz, J. Spatiotemporal Analysis of the Surface Urban Heat Island (SUHI), Air Pollution and Disease Pattern: An Applied Study on the City of Granada (Spain). *Environ. Sci. Pollut. Res.* **2023**, *30*, 57617–57637. [[CrossRef](#)]
- Bradford, K.; Abrahams, L.; Hegglin, M.; Klima, K. A Heat Vulnerability Index and Adaptation Solutions for Pittsburgh, Pennsylvania. *Environ. Sci. Technol.* **2015**, *49*, 11303–11311. [[CrossRef](#)]
- Nwakaire, C.M.; Onn, C.C.; Yap, S.P.; Yuen, C.W.; Onodagu, P.D. Urban Heat Island Studies with Emphasis on Urban Pavements: A Review. *Sustain. Cities Soc.* **2020**, *63*, 102476. [[CrossRef](#)]
- Li, W.; Bai, Y.; Chen, Q.; He, K.; Ji, X.; Han, C. Discrepant Impacts of Land Use and Land Cover on Urban Heat Islands: A Case Study of Shanghai, China. *Ecol. Indic.* **2014**, *47*, 171–178. [[CrossRef](#)]
- Deilami, K.; Kamruzzaman, M.; Liu, Y. Urban Heat Island Effect: A Systematic Review of Spatio-Temporal Factors, Data, Methods, and Mitigation Measures. *Int. J. Appl. Earth Obs. Geoinf.* **2018**, *67*, 30–42. [[CrossRef](#)]
- Zheng, B.; Myint, S.W.; Fan, C. Spatial Configuration of Anthropogenic Land Cover Impacts on Urban Warming. *Landsc. Urban Plan.* **2014**, *130*, 104–111. [[CrossRef](#)]
- Kim, S.W.; Brown, R.D. Urban Heat Island (UHI) Intensity and Magnitude Estimations: A Systematic Literature Review. *Sci. Total Environ.* **2021**, *779*, 146389. [[CrossRef](#)]
- Ivajnsič, D.; Kaligarič, M.; Žiberna, I. Geographically Weighted Regression of the Urban Heat Island of a Small City. *Appl. Geogr.* **2014**, *53*, 341–353. [[CrossRef](#)]
- Santamouris, M. Heat Island Research in Europe: The State of the Art. *Adv. Build. Energy Res.* **2007**, *1*, 123–150. [[CrossRef](#)]
- Sun, Y.; Wang, S.; Wang, Y. Estimating Local-Scale Urban Heat Island Intensity Using Nighttime Light Satellite Imageries. *Sustain. Cities Soc.* **2020**, *57*, 102125. [[CrossRef](#)]
- Oke, T.R.; Mills, G.; Christen, A.; Voogt, J.A. *Urban Climates*; Cambridge University Press: Cambridge, UK, 2017. [[CrossRef](#)]
- Rizwan, A.M.; Dennis, L.Y.C.; Liu, C. A Review on the Generation, Determination and Mitigation of Urban Heat Island. *J. Environ. Sci.* **2008**, *20*, 120–128. [[CrossRef](#)]
- Zhou, W.; Qian, Y.; Li, X.; Li, W.; Han, L. Relationships between Land Cover and the Surface Urban Heat Island: Seasonal Variability and Effects of Spatial and Thematic Resolution of Land Cover Data on Predicting Land Surface Temperatures. *Landsc. Ecol.* **2014**, *29*, 153–167. [[CrossRef](#)]
- Martin-Vide, J.; Moreno-García, M.C. Probability Values for the Intensity of Barcelona’s Urban Heat Island (Spain). *Atmos. Res.* **2020**, *240*, 104877. [[CrossRef](#)]
- Chang, Y.; Xiao, J.; Li, X.; Froking, S.; Zhou, D.; Schneider, A.; Weng, Q.; Yu, P.; Wang, X.; Li, X.; et al. Exploring Diurnal Cycles of Surface Urban Heat Island Intensity in Boston with Land Surface Temperature Data Derived from GOES-R Geostationary Satellites. *Sci. Total Environ.* **2021**, *763*, 144224. [[CrossRef](#)]
- Siddiqui, A.; Kushwaha, G.; Nikam, B.; Srivastav, S.K.; Shelar, A.; Kumar, P. Analysing the Day/Night Seasonal and Annual Changes and Trends in Land Surface Temperature and Surface Urban Heat Island Intensity (SUHII) for Indian Cities. *Sustain. Cities Soc.* **2021**, *75*, 103374. [[CrossRef](#)]
- Deng, X.; Yu, W.; Shi, J.; Huang, Y.; Li, D.; He, X.; Zhou, W.; Xie, Z. Characteristics of Surface Urban Heat Islands in Global Cities of Different Scales: Trends and Drivers. *Sustain. Cities Soc.* **2024**, *107*, 105483. [[CrossRef](#)]
- Du, J.; Xiang, X.; Zhao, B.; Zhou, H. Impact of Urban Expansion on Land Surface Temperature in Fuzhou, China Using Landsat Imagery. *Sustain. Cities Soc.* **2020**, *61*, 102346. [[CrossRef](#)]
- Chen, F.; Yang, S.; Yin, K.; Chan, P. Challenges to Quantitative Applications of Landsat Observations for the Urban Thermal Environment. *J. Environ. Sci. (China)* **2017**, *59*, 80–88. [[CrossRef](#)]
- Aslan, N.; Koc-San, D. Analysis of Relationship between Urban Heat Island Effect and Land Use/Cover Type Using Landsat 7 ETM+ and Landsat 8 OLI Images. In *International Archives of the Photogrammetry, Remote Sensing and Spatial Information Sciences—ISPRS Archives*; International Society for Photogrammetry and Remote Sensing: Bethesda, MD, USA, 2016; Volume 41, pp. 821–828. [[CrossRef](#)]

24. Lemus-Canovas, M.; Martin-Vide, J.; Moreno-Garcia, M.C.; Lopez-Bustins, J.A. Estimating Barcelona's Metropolitan Daytime Hot and Cold Poles Using Landsat-8 Land Surface Temperature. *Sci. Total Environ.* **2020**, *699*, 134307. [[CrossRef](#)] [[PubMed](#)]
25. Yuan, F.; Bauer, M.E. Comparison of Impervious Surface Area and Normalized Difference Vegetation Index as Indicators of Surface Urban Heat Island Effects in Landsat Imagery. *Remote Sens. Environ.* **2007**, *106*, 375–386. [[CrossRef](#)]
26. Guo, A.; Yang, J.; Sun, W.; Xiao, X.; Cecilia, J.X.; Jin, C.; Li, X. Impact of Urban Morphology and Landscape Characteristics on Spatiotemporal Heterogeneity of Land Surface Temperature. *Sustain. Cities Soc.* **2020**, *63*, 102443. [[CrossRef](#)]
27. Hidalgo-García, D.; Arco-Díaz, J. Modeling the Surface Urban Heat Island (SUHI) to Study of Its Relationship with Variations in the Thermal Field and with the Indices of Land Use in the Metropolitan Area of Granada (Spain). *Sustain. Cities Soc.* **2022**, *87*, 104166. [[CrossRef](#)]
28. Oliveira, A.; Lopes, A.; Niza, S. Local Climate Zones in Five Southern European Cities: An Improved GIS-Based Classification Method Based on Copernicus Data. *Urban Clim.* **2020**, *33*, 100631. [[CrossRef](#)]
29. Mirchooli, F.; Sadeghi, S.H.; Darvishan, A.K. Analyzing Spatial Variations of Relationships between Land Surface Temperature and Some Remotely Sensed Indices in Different Land Uses. *Remote Sens. Appl. Soc. Environ.* **2020**, *19*, 100359. [[CrossRef](#)]
30. Salvati, A.; Coch, H.; Morganti, M. Effects of Urban Compactness on the Building Energy Performance in Mediterranean Climate. In *Energy Procedia*; Elsevier Ltd.: Amsterdam, The Netherlands, 2017; Volume 122, pp. 499–504. [[CrossRef](#)]
31. Tepanosyan, G.; Muradyan, V.; Hovsepyan, A.; Pinigin, G.; Medvedev, A.; Asmaryan, S. Studying Spatial-Temporal Changes and Relationship of Land Cover and Surface Urban Heat Island Derived through Remote Sensing in Yerevan, Armenia. *Build. Environ.* **2021**, *187*, 107390. [[CrossRef](#)]
32. Oke, T.R. The Energetic Basis of the Urban Heat Island. *Q. J. R. Met. Soc.* **1982**, *108*, 551. [[CrossRef](#)]
33. Bala, R.; Prasad, R.; Yadav, V.P. A Comparative Analysis of Day and Night Land Surface Temperature in Two Semi-Arid Cities Using Satellite Images Sampled in Different Seasons. *Adv. Space Res.* **2020**, *66*, 412–425. [[CrossRef](#)]
34. Chen, H.; Deng, Q.; Zhou, Z.; Ren, Z.; Shan, X. Influence of Land Cover Change on Spatio-Temporal Distribution of Urban Heat Island—A Case in Wuhan Main Urban Area. *Sustain. Cities Soc.* **2022**, *79*, 103715. [[CrossRef](#)]
35. Salvati, A.; Roura, H.C.; Cecere, C. Assessing the Urban Heat Island and Its Energy Impact on Residential Buildings in Mediterranean Climate: Barcelona Case Study. *Energy Build.* **2017**, *146*, 38–54. [[CrossRef](#)]
36. Dienst, M.; Lindén, J.; Saladié, Ò.; Esper, J. Detection and Elimination of UHI Effects in Long Temperature Records from Villages—A Case Study from Tivissa, Spain. *Urban Clim.* **2019**, *27*, 372–383. [[CrossRef](#)]
37. Barrao, S.; Serrano-Notivoli, R.; Cuadrat, J.M.; Tejedor, E.; Sánchez, M.A.S. Characterization of the UHI in Zaragoza (Spain) Using a Quality-Controlled Hourly Sensor-Based Urban Climate Network. *Urban Clim.* **2022**, *44*, 101207. [[CrossRef](#)]
38. Vicente-Serrano, S.M.; Cuadrat-Prats, J.M.; Saz-Sánchez, M.A. Spatial Patterns of the Urban Heat Island in Zaragoza (Spain). *Clim. Res.* **2005**, *30*, 61–69. [[CrossRef](#)]
39. Alonso, M.S.; Fidalgo, M.R.; Labajo, J.L. The Urban Heat Island in Salamanca (Spain) and Its Relationship to Meteorological Parameters. *Clim. Res.* **2007**, *34*, 39–46. [[CrossRef](#)]
40. Gago, E.J.; Berrizbeitia, S.E.; Torres, R.P.; Muneer, T. Effect of Land Use/Cover Changes on Urban Cool Island Phenomenon in Seville, Spain. *Energies* **2020**, *13*, 3040. [[CrossRef](#)]
41. Acero, J.A.; Arrizabalaga, J.; Kupski, S.; Katzschner, L. Urban Heat Island in a Coastal Urban Area in Northern Spain. *Theor. Appl. Climatol.* **2013**, *113*, 137–154. [[CrossRef](#)]
42. Senciales-González, J.M.; Rodrigo-Comino, J.; Smith, P. Surveying Topographical Changes and Climate Variations to Detect the Urban Heat Island in the City of Málaga (Spain). *Geogr. Res. Lett.* **2020**, *46*, 521–543. [[CrossRef](#)]
43. Hidalgo-García, D.; Arco-Díaz, J. Space-Time Analysis of the Earth's Surface Temperature, Surface Urban Heat Island and Urban Hotspot: Relationships with Variation of the Thermal Field in Andalusia (Spain). *Urban Ecosyst.* **2023**, *26*, 525–546. [[CrossRef](#)]
44. Moreno, H.L.; Sánchez, S.-G.; López, M.E.R.; González, F.J.N. Thermal Characterization of Urban Heat Island (UHI) According to Urban Morphology of Madrid. In Proceedings of the III International Congress on Construction and Building Research, Madrid, Spain, 14–16 December 2015.
45. Lehoczky, A.; Sobrino, J.; Skoković, D.; Aguilar, E. The Urban Heat Island Effect in the City of Valencia: A Case Study for Hot Summer Days. *Urban Sci.* **2017**, *1*, 9. [[CrossRef](#)]
46. Quereda, J.; Montón, E.; Quereda, V.; Mollá, B. Significant Climate Warming (1950–2013) in the Spanish Mediterranean: Natural Trend or Urban Heat Island (UHI). *Tethys* **2016**, *2016*, 11–20. [[CrossRef](#)]
47. Quereda Sala, J.; Montón Chiva, E.; Quereda Vázquez, M.V.; Mollà Cantavella, B. The Urban Effect (UHI) in Spanish Mediterranean. *Wulfenia* **2015**, *22*, 89–100.
48. World Bank Group. Urban Population (% of Total Population)—Spain. 2024. Available online: <https://data.worldbank.org/indicator/SP.URB.TOTL.IN.ZS?locations=ES> (accessed on 19 June 2024).
49. Jato-Espino, D. Spatiotemporal Statistical Analysis of the Urban Heat Island Effect in a Mediterranean Region. *Sustain. Cities Soc.* **2019**, *46*, 101427. [[CrossRef](#)]
50. Chen, X.; Zhang, Y. Impacts of Urban Surface Characteristics on Spatiotemporal Pattern of Land Surface Temperature in Kunming of China. *Sustain. Cities Soc.* **2017**, *32*, 87–99. [[CrossRef](#)]
51. Quereda, J.; Montón, E.; Quereda, V. Climate Warming in the Spanish Mediterranean: Its Magnitude and Nature. *Tethys* **2020**, *2020*, 1–9. [[CrossRef](#)]

52. CNIG. Work from Orto-AMS 1956–1957 CC-BY 4.0 Scne.Es. Available online: <https://centrodedescargas.cnig.es/CentroDescargas/index.jsp> (accessed on 21 February 2019).
53. CNIG. Work from PNOAHISTORICO 2004–2022 CC-BY 4.0 Scne.Es. Available online: <https://centrodedescargas.cnig.es/CentroDescargas/index.jsp> (accessed on 21 February 2019).
54. Rocafort, C.; Dalmau, C.; Chias Carbó, B. *España Regional. Planos*; Alberto Martín: Barcelona, Spain, 1910; Volume 3.
55. INE. Municipality Population. 2023. Available online: <https://www.ine.es/dynt3/inebase/index.htm?padre=525> (accessed on 3 April 2024).
56. Copernicus Land Monitoring Service. CORINE Land Cover 1990 (Vector/Raster 100 m), Europe, 6-Yearly CC-BY 4.0 Scne.Es. Available online: <https://centrodedescargas.cnig.es/CentroDescargas/index.jsp#> (accessed on 22 February 2024). [[CrossRef](#)]
57. Copernicus Land Monitoring Service. CORINE Land Cover 2018 (Vector/Raster 100 m), Europe, 6-Yearly. CC-BY 4.0 Scne.Es. Available online: <https://centrodedescargas.cnig.es/CentroDescargas/index.jsp#> (accessed on 22 February 2024). [[CrossRef](#)]
58. Copernicus. CORINE Land Cover Nomenclature Guidelines. 2024. Available online: <https://land.copernicus.eu/content/corine-land-cover-nomenclature-guidelines/html/> (accessed on 21 February 2024).
59. Climate Engine Team. Dataset Information, Landsat NDVI. Available online: <https://support.climateengine.org/article/104-datatasetsinfo> (accessed on 11 July 2024).
60. Huntington, J.L.; Hegewisch, K.C.; Daudert, B.; Morton, C.G.; Abatzoglou, J.T.; McEvoy, D.J.; Erickson, T. Climate Engine: Cloud Computing and Visualization of Climate and Remote Sensing Data for Advanced Natural Resource Monitoring and Process Understanding. *Bull. Am. Meteorol. Soc.* **2017**, *98*, 2397–2409. [[CrossRef](#)]
61. Desert Research Institute and University of California Merced. Climate Engine, Version 2.1. (1985–2023). Available online: <http://climateengine.org> (accessed on 20 March 2024).
62. Ravanelli, R.; Nascetti, A.; Cirigliano, R.V.; Rico, C.D.; Leuzzi, G.; Monti, P.; Crespi, M. Monitoring the Impact of Land Cover Change on Surface Urban Heat Island through Google Earth Engine: Proposal of a Global Methodology, First Applications and Problems. *Remote Sens.* **2018**, *10*, 1488. [[CrossRef](#)]
63. Kumar, L.; Mutanga, O. Google Earth Engine Applications Since Inception: Usage, Trends, and Potential. *Remote Sens.* **2018**, *10*, 1509. [[CrossRef](#)]
64. Amani, M.; Ghorbanian, A.; Ahmadi, S.A.; Kakooei, M.; Moghimi, A.; Mirmazloumi, S.M.; Moghaddam, S.H.A.; Mahdavi, S.; Ghahremanloo, M.; Parsian, S.; et al. Google Earth Engine Cloud Computing Platform for Remote Sensing Big Data Applications: A Comprehensive Review. *IEEE J. Sel. Top. Appl. Earth Obs. Remote Sens.* **2020**, *13*, 5326–5350. [[CrossRef](#)]
65. Wang, L.; Diao, C.; Xian, G.; Yin, D.; Lu, Y.; Zou, S.; Erickson, T.A. A Summary of the Special Issue on Remote Sensing of Land Change Science with Google Earth Engine. *Remote Sens. Environ.* **2020**, *248*, 112002. [[CrossRef](#)]
66. Gorelick, N.; Hancher, M.; Dixon, M.; Ilyushchenko, S.; Thau, D.; Moore, R. Google Earth Engine: Planetary-Scale Geospatial Analysis for Everyone. *Remote Sens. Environ.* **2017**, *202*, 18–27. [[CrossRef](#)]
67. Zhang, H.; Yin, Y.; An, H.; Lei, J.; Li, M.; Song, J.; Han, W. Surface Urban Heat Island and Its Relationship with Land Cover Change in Five Urban Agglomerations in China Based on GEE. *Environ. Sci. Pollut. Res.* **2022**, *29*, 82271–82285. [[CrossRef](#)]
68. Purio, M.A.; Yoshitake, T.; Cho, M. Assessment of Intra-Urban Heat Island in a Densely Populated City Using Remote Sensing: A Case Study for Manila City. *Remote Sens.* **2022**, *14*, 5573. [[CrossRef](#)]
69. Rejuso, A.M.; Cortes, A.C.; Blanco, A.C.; Cruz, C.A.; Babaan, J.B. Spatio-Temporal Analysis of Urban Heat Island in Mandaue City, Philippines. In *International Archives of the Photogrammetry, Remote Sensing and Spatial Information Sciences—ISPRS Archives*; International Society for Photogrammetry and Remote Sensing: Bethesda, MD, USA, 2019; Volume 42, pp. 361–367. [[CrossRef](#)]
70. Ravanelli, R.; Nascetti, A.; Cirigliano, V.; Rico, C.D.; Leuzzi, G.; Monti, P.; Crespi, M. Monitoring of the Urban Heat Island through Google Earth Engine: A Global Methodology and Its Application to Different Cities of the United States. *Int. Arch. Photogramm. Remote Sens. Spat. Inf. Sci.* **2018**, *XLII-3*, 1467–1472. [[CrossRef](#)]
71. Gkatzioura, P.E.; Perakis, K. Analysis of Urban Heat Island (UHI) through Climate Engine and ARCGIS PRO in Different Cities of Bulgaria. In *Proceedings of the Eighteenth International Scientific Conference, Virtual Event*, 24–27 June 2022.
72. CNIG. Download Center. Available online: <https://centrodedescargas.cnig.es/CentroDescargas/index.jsp> (accessed on 15 January 2024).
73. Stal, C.; Sloover, L.D.; Verbeurgt, J.; Wulf, A.D. On Finding a Projected Coordinate Reference System. *Geographies* **2022**, *2*, 245–257. [[CrossRef](#)]
74. Climate Engine Team. On-Demand Insights from Climate and Earth Observations Data. 2024. Available online: <https://www.climateengine.org/> (accessed on 20 March 2024).
75. Mejjad, N.; Rossi, A.; Pavel, A.B. The Coastal Tourism Industry in the Mediterranean: A Critical Review of the Socio-Economic and Environmental Pressures & Impacts. *Tour. Manag. Perspect.* **2022**, *44*, 101007. [[CrossRef](#)]
76. Masot, A.N.; Alonso, G.C.; Moriche, Á.E. Spatial Analysis of the Rural-Urban Structure of the Spanish Municipalities. *ISPRS Int. J. Geo-Inf.* **2020**, *9*, 213. [[CrossRef](#)]
77. Jiménez-Olivencia, Y.; Ibáñez-Jiménez, Á.; Porcel-Rodríguez, L.; Zimmerer, K. Land Use Change Dynamics in Euro-Mediterranean Mountain Regions: Driving Forces and Consequences for the Landscape. *Land Use Policy* **2021**, *109*, 105721. [[CrossRef](#)]
78. López Ortiz, M.I.; Melgarejo Moreno, J. Evolución Histórica de La Agricultura de La Provincia de Alicante, 1900–2000. In *Libro Jubilar en Homenaje al Profesor Antonio Gil Olcina. Edición ampliada*; Servicio de Publicaciones de la Universidad de Alicante: Alicante, Spain, 2016; pp. 1063–1085. [[CrossRef](#)]

79. Hrushka, V.V.; Horozhankina, N.A.; Boyko, Z.V.; Korneyev, M.V.; Nebaba, N.A. Transport Infrastructure of Spain as a Factor in Tourism Development. *J. Geol. Geogr. Geocol.* **2021**, *30*, 429–440. [[CrossRef](#)]
80. Martí, P.; García-Mayor, C. The Huerta Agricultural Landscape in the Spanish Mediterranean Arc: One Landscape, Two Perspectives, Three Specific Huertas. *Land* **2020**, *9*, 460. [[CrossRef](#)]
81. McCormick, M.P.; Thomason, L.W.; Trepte, C.R. Atmospheric Effects of the Mt Pinatubo Eruption. *Nature* **1995**, *373*, 399–404. [[CrossRef](#)]
82. Medhaug, I.; Stolpe, M.B.; Fischer, E.M.; Knutti, R. Reconciling Controversies about the “Global Warming Hiatus”. *Nature* **2017**, *545*, 41–47. [[CrossRef](#)] [[PubMed](#)]
83. Buyantuyev, A.; Wu, J. Urban Heat Islands and Landscape Heterogeneity: Linking Spatiotemporal Variations in Surface Temperatures to Land-Cover and Socioeconomic Patterns. *Landsc. Ecol.* **2010**, *25*, 17–33. [[CrossRef](#)]
84. Founda, D.; Pierros, F.; Petrakis, M.; Zerefos, C. Interdecadal Variations and Trends of the Urban Heat Island in Athens (Greece) and Its Response to Heat Waves. *Atmos. Res.* **2015**, *161–162*, 1–13. [[CrossRef](#)]
85. Giannaros, T.M.; Melas, D. Study of the Urban Heat Island in a Coastal Mediterranean City: The Case Study of Thessaloniki, Greece. *Atmos. Res.* **2012**, *118*, 103–120. [[CrossRef](#)]
86. Montaner-Fernández, D.; Morales-Salinas, L.; Rodriguez, J.S.; Cárdenas-Jirón, L.; Huete, A.; Fuentes-Jaque, G.; Pérez-Martínez, W.; Cabezas, J. Spatio-Temporal Variation of the Urban Heat Island in Santiago, Chile during Summers 2005–2017. *Remote Sens.* **2020**, *12*, 3345. [[CrossRef](#)]
87. MacLachlan, A.; Biggs, E.; Roberts, G.; Boruff, B. Urbanisation-Induced Land Cover Temperature Dynamics for Sustainable Future Urban Heat Island Mitigation. *Urban Sci.* **2017**, *1*, 38. [[CrossRef](#)]
88. Bahi, H.; Rhinane, H.; Bensalmia, A.; Fehrenbach, U.; Scherer, D. Effects of Urbanization and Seasonal Cycle on the Surface Urban Heat Island Patterns in the Coastal Growing Cities: A Case Study of Casablanca, Morocco. *Remote Sens.* **2016**, *8*, 829. [[CrossRef](#)]
89. Evola, G.; Gagliano, A.; Fichera, A.; Marletta, L.; Martinico, F.; Nocera, F.; Pagano, A. UHI Effects and Strategies to Improve Outdoor Thermal Comfort in Dense and Old Neighbourhoods. In *Energy Procedia*; Elsevier Ltd.: Amsterdam, The Netherlands, 2017; Volume 134, pp. 692–701. [[CrossRef](#)]
90. Yenneti, K.; Ding, L.; Prasad, D.; Ulpiani, G.; Paolini, R.; Haddad, S.; Santamouris, M. Urban Overheating and Cooling Potential in Australia: An Evidence-Based Review. *Climate* **2020**, *8*, 126. [[CrossRef](#)]
91. Lai, J.; Zhan, W.; Voogt, J.; Quan, J.; Huang, F.; Zhou, J.; Bechtel, B.; Hu, L.; Wang, K.; Cao, C.; et al. Meteorological Controls on Daily Variations of Nighttime Surface Urban Heat Islands. *Remote Sens. Environ.* **2021**, *253*, 112198. [[CrossRef](#)]
92. Elshater, A.; Abusaada, H.; Alfiky, A.; El-Bardisy, N.; Elmarakby, E.; Grant, S. Workers’ Satisfaction Vis-à-Vis Environmental and Socio-Morphological Aspects for Sustainability and Decent Work. *Sustainability* **2022**, *14*, 1699. [[CrossRef](#)]
93. Zhang, Y.; Teoh, B.K.; Zhang, L. Multi-Objective Optimization for Energy-Efficient Building Design Considering Urban Heat Island Effects. *Appl. Energy* **2024**, *376*, 124117. [[CrossRef](#)]

Disclaimer/Publisher’s Note: The statements, opinions and data contained in all publications are solely those of the individual author(s) and contributor(s) and not of MDPI and/or the editor(s). MDPI and/or the editor(s) disclaim responsibility for any injury to people or property resulting from any ideas, methods, instructions or products referred to in the content.